

1           Quasi-consistent efficient meshfree thin shell  
2       formulation with naturally stabilized enforced essential  
3           boundary conditions

4           Junchao Wu<sup>a,\*</sup>, Yangtao Xu<sup>a</sup>, Bin Xu<sup>a</sup>, Syed Humayun Basha<sup>a</sup>

<sup>a</sup>*Key Laboratory for Intelligent Infrastructure and Monitoring of Fujian Province, Key Laboratory for Structural Engineering and Disaster Prevention of Fujian Province, College of Civil Engineering, Huaqiao University, Xiamen, Fujian, 361021, China*

---

5           **Abstract**

This research proposed an efficient and quasi-consistent meshfree thin shell formulation with naturally stabilized enforcement of essential boundary conditions. Within the framework of the Hu-Washizu variational principle, a mixed formulation of displacements, strains and stresses is employed in this approach, where the displacements are discretized using meshfree shape functions, and the strains and stresses are expressed using smoothed gradients and covariant bases. The smoothed gradients satisfy the first second-order integration constraint and observed variational consistency for polynomial strains and stresses. Owing to Hu-Washizu variational principle, the essential boundary conditions automatically arise in its weak form. As a result, the suggested technique's enforcement of essential boundary conditions resembles that of the traditional Nitsche's method. Contrary to Nitsche's method, the costly higher order derivatives of conventional meshfree shape functions are replaced by the smoothed gradients with fast computation, which improve the efficiency. Meanwhile, the proposed formulation features a naturally stabilized term without adding any artificial stabilization factors, which eliminates the application of penalty method as a stabilization. Further, the efficacy of the proposed Hu-Washizu meshfree thin shell formulation is illustrated by a set of classical standard thin shell problems.

6           *Keywords:* Meshfree, Thin shell, Hu-Washizu variational principle,  
7           Reproducing kernel gradient smoothing, Essential boundary condition

---

---

\*Corresponding author  
Email address: jcwu@hqu.edu.cn (Junchao Wu)

8      **1. Introduction**

9      Thin shell structures generally adhere to the Kirchhoff hypothesis [1], that  
10     neglects the shear deformation can be described using Galerkin formulation  
11     which requires to have at least  $C^1$  continuity. The traditional Traditional finite  
12     element methods usually have typically employ  $C^0$  continuous shape functions,  
13     and it prefers Mindlin thick shear theory, hybrid and mixed models, like linear  
14     and nonlinear Mindlin model [2, 3] and the one inextensible director model [4],  
15     in simulation of shell structure[3]. Meshfree methods [17, 18, 11]. Over the past  
16     thirty years, various novel formulations with high order smoothed shape functions  
17     have garnered much research attention over the past thirty years. These  
18     techniques been applied to thin shell formulations. These include element-free  
19     Galerkin method [5], maximum-entropy method [6], Hermite reproducing kernel  
20     particle method [7], peridynamics [8], isogeometric [9], and others. For a more  
21     comprehensive review of advances and applications of meshfree techniques in  
22     various scientific and engineering fields, refer to [10, 11, 12, 13, 14, 15, 16, 16].  
23     Among these approaches, Galerkin meshfree methods with moving least square  
24     approximation (MLS) [17] or reproducing kernel approximation (RK) [18] es-  
25     tablished the shape functions based on a collection of dispersed nodes, and high  
26     order continuity of shape functions can be easily achieved even with low-order  
27     basis functions. For thin shell analysis, high order meshfree approximation can  
28     also further alleviate the membrane locking caused by the mismatched approxi-  
29     mation order of membrane strain and bending strain [5]. Moreover, nodal-based  
30     meshfree node-based MLS/RK approximations generally offer the flexibility of  
31     local refinement and can relieve the burden of mesh distortion. Owing to these  
32     benefits, numerous meshfree techniques have been developed and implemented  
33     in many scientific and engineering fields [10? , 6, 14, 13, 15, 16]. However, the  
34     high order smoothed meshfree shape functions accompany the enlarged and  
35     overlapping supports, which may potentially cause many problems for shape  
36     functions. One of the issues is the loss of the Kronecker delta property, which  
37     means that, unlike the finite element methods, the necessary boundary con-  
38     ditions cannot be directly enforced [19]. Another issue is that the variational  
39     consistency or said integration constraint, which is a condition that requires the  
40     formulation to exactly reproduce the solution spanned by the basis functions,  
41     cannot be satisfied. This issue is mainly caused by the misalignment between  
42     the numerical integration domains and supports of shape functions. Thus, the  
43     shape functions exhibit a piecewise nature in each integration domain. Besides,  
44     it has to be noted that the traditional integration rules like Gauss scheme can-  
45     not ensure the integration accuracy in Galerkin weak form [20, 21]. Therefore,  
46     variational consistency is vital to the solution accuracy in the Galerkin meshfree  
47     formulations.

48      Various ways have been presented to enforce the necessary boundary for  
49     Galerkin meshfree methods directly, including the boundary singular kernel  
50     method [22], mixed transformation method [22], and interpolation element-free  
51     method [23] for recovering shape functions' Kronecker property. However, these  
52     methods were not based on variational setting and cannot guarantee varia-

tional consistency. ~~In the absence of a meshfree node, accuracy enforcement might be poor. The accuracy maybe poor at locations away from the sample points.~~ In contrast, enforcing the essential boundary conditions using a variational approach is preferred for Galerkin meshfree methods. The variational consistent Lagrange multiplier approach was initially used to the Galerkin meshfree method by Belytschko et al. [17]. In this method, the extra degrees of freedom are used to determine the discretion of Lagrange multiplier. Ivannikov et al. [24] extended this approach to geometrically nonlinear thin shells. Lu et al. [25] suggested the modified variational essential boundary enforcement approach and expressed the Lagrange multiplier by equivalent tractions to eliminate the excess degrees of freedom. However, the coercivity of this approach is not always ensured and potentially reduces the accuracy. Zhu and Atluri [26] pioneered the penalty method for meshfree method, making it a straightforward approach to enforce essential boundary conditions via Galerkin weak form. However, the penalty method lacks variational consistency and requires experimental artificial parameters whose optimal value is hard to determine. Fernández-Méndez and Huerta [19] imposed necessary boundary conditions using Nitsche's approach in the meshfree formulation. This approach can be seen as a hybrid combination of the modified variational method and the penalty method because the modified variational method generates variational consistency through the use of a consistent term, and the penalty method is used as a stabilized term to recover the coercivity. Skatulla and Sansour [27] extended Nitsche's thin shell analysis method and proposed an iteration algorithm to determine artificial parameters at each integration point. ~~In addition, the Nitsche's method has been successful used in multiple patches problems [28] and composited material problems [29] to maintain the variational consistency between different geometrical or material domains.~~

In order to address the issue of numerical integration, a series of consistent integration schemes have been developed for Galerkin meshfree methods. Among these include stabilized conforming nodal integration [30], variational consistent integration [31], quadratic consistent integration [32], reproducing kernel gradient smoothing integration [33], and consistent projection integration [34]. The assumed strain approach establishes the most consistent integration scheme, while the smoothed gradient replaces the costly higher order derivatives of traditional meshfree shape functions and shows a high efficiency. Moreover, to achieve global variational consistency, a consistent essential boundary condition enforcement must be combined with the consistent integration scheme. The combination of consistent integration scheme and Nitsche's method for treating essential boundary conditions may demonstrate better performance since both the methods can satisfy the coercivity without requiring additional degrees of freedom. Nevertheless, Nitsche's approach still retains the artificial parameters in the stabilized terms, and it is essential to remain cautious of the costly higher order derivatives, particularly for thin plate and thin shell problems. Recently, Wu et al. [35, 36] proposed an efficient and stabilized essential boundary condition enforcement method based upon the Hellinger-Reissner variational principle, where a mixed formulation in Hellinger-Reissner weak form recasts the

99 reproducing kernel gradient smoothing integration. The terms required for enforcing  
100 essential boundary conditions are identical to the Nitsche's method, and both have consistent and stabilized terms.  
101 However, the stabilized term of this method naturally exists in the Hellinger-Reissner weak form and no longer needs  
102 the artificial parameters, even for essential boundary enforcement. Instead all  
103 of the higher order derivatives are represented by the smoothed gradients and  
104 their derivatives.

105 In this study, an efficient and stabilized variational consistent meshfree  
106 method that naturally enforces the essential boundary conditions is developed  
107 for thin shell structures. Following the concept of the Hellinger-Reissner principle  
108 base consistent meshfree method, the Hu-Washizu variational principle of  
109 complementary energy with variables of displacement, strains, and stresses were  
110 employed. The displacement is approximated by conventional meshfree shape  
111 functions, and the strains and stresses were expressed by smoothed gradients  
112 with covariant bases. It is important to note that although the first second-order  
113 integration requirements were naturally embedded in the smoothed gradients,  
114 their fulfillment resulted in a quasi-satisfaction of variational consistency. This  
115 is mainly because of the non-polynomial nature of the stresses. Hu-Washizu's  
116 weak form was used to evaluate all the essential boundary conditions regarding  
117 displacements and rotations. This type of formulation is similar to the  
118 Nitsche's method but does not require any artificial parameters. Compared  
119 with Nitsche's method, conventional reproducing smoothed gradients and its  
120 direct derivatives replace the costly higher order derivatives. By utilizing the  
121 advantages of a replicating kernel gradient smoothing framework, the smoothed  
122 gradients showed better performance compared to conventional derivatives of  
123 shape functions, hence increasing the meshfree formulation's computational ef-  
124 ficiency.

125 The remainder of this research article is structured as follows: The kinematics  
126 of the thin shell structure and the weak form of the associated Hu-Washizu  
127 principle are briefly described in Section 2. The mixed formulation regarding  
128 the displacements, strains and stresses in accordance with Hu-Washizu weak  
129 form are presented in Section 3. The discrete equilibrium equations are derived  
130 in Section 4 using the naturally occurring accommodation of essential. Subse-  
131 quently, they are compared to the equations obtained using Nitsche's method.  
132 The numerical results in Section 5 validate the efficacy of the proposed Hu-  
133 Washizu meshfree thin shell formulation. Lastly, the concluding remarks are  
134 presented in Section 6.

136    **2. Hu-Washizu's formulation of complementary energy for thin shell**

137    *2.1. Kinematics for thin shell*

138    Consider the configuration of a shell  $\bar{\Omega}$ , as shown in Fig. 1, which can be  
 139    easily described by a parametric curvilinear coordinate system  $\xi = \{\xi^i\}_{i=1,2,3}$ .  
 140    The mid-surface of the shell denoted by  $\Omega$  is specified by the in-plane coordinates  
 141     $\xi = \{\xi^\alpha\}_{\alpha=1,2}$ , as the thickness direction of shell is by  $\xi^3$ ,  $-\frac{h}{2} \leq \xi^3 \leq \frac{h}{2}$ ,  $h$  is  
 142    the thickness of shell. In this work, Latin indices take the values from 1 to 3,  
 143    and Greek indices are evaluated by 1 or 2. For the Kirchhoff hypothesis [5], the  
 144    position  $\mathbf{x} \in \bar{\Omega}$  is defined by linear functions with respect to  $\xi^3$  :

$$\mathbf{x}(\xi^1, \xi^2, \xi^3) = \mathbf{r}(\xi^1, \xi^2) + \xi^3 \mathbf{a}_3(\xi^1, \xi^2) \quad (1)$$

in which  $\mathbf{r}$  means the position on the mid-surface of shell, and  $\mathbf{a}_3$  is correspond-

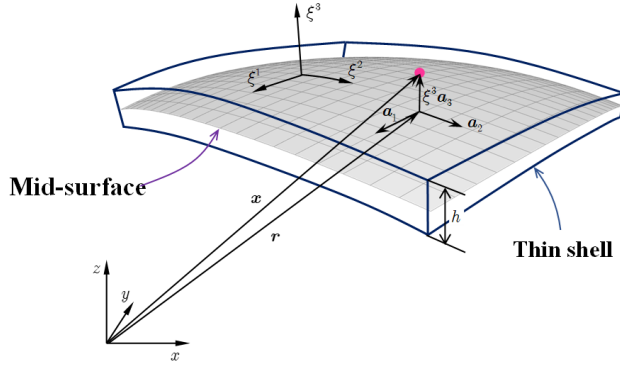


Figure 1: Kinematics for thin shell.

145  
 146    ing normal direction. For the mid-surface of shell, the in-plane covariant base  
 147    vector with respect to  $\xi^\alpha$  can be derived by a trivial partial differentiation to  $\mathbf{r}$ :

$$\mathbf{a}_\alpha = \frac{\partial \mathbf{r}}{\partial \xi^\alpha} = \mathbf{r}_{,\alpha}, \alpha = 1, 2 \quad (2)$$

148    to provide for a clear expression, the subscript comma denotes the partial dif-  
 149    ferentiation operation with respect to in-plane coordinates  $\xi^\alpha$ , and the normal  
 150    vector  $\mathbf{a}_3$  can be obtained by the normalized cross product of  $\mathbf{a}_\alpha$ 's as follows:

$$\mathbf{a}_3 = \frac{\mathbf{a}_1 \times \mathbf{a}_2}{\|\mathbf{a}_1 \times \mathbf{a}_2\|} \quad (3)$$

151    where  $\|\bullet\|$  is the Euclidean norm operator.

152    With the assumption of infinitesimal deformation, the strain components  
 153    with respect to the global contravariant base can be stated as:

$$\epsilon_{ij} = \frac{1}{2} (\mathbf{x}_{,i} \cdot \mathbf{u}_{,j} + \mathbf{u}_{,i} \cdot \mathbf{x}_{,j}) \quad (4)$$

<sup>154</sup> where  $\mathbf{u}$  represents the displacement for the shell deformation. To satisfy the  
<sup>155</sup> Kirchhoff hypothesis, the displacement is assumed to be of the following form:

$$\mathbf{u}(\xi^1, \xi^2, \xi^3) = \mathbf{v}(\xi^1, \xi^2) + \boldsymbol{\theta}(\xi^1, \xi^2)\xi^3 \quad (5)$$

<sup>156</sup> in which the quadratic and higher order terms are neglected.  $\mathbf{v}, \boldsymbol{\theta}$  represent  
<sup>157</sup> the displacement and rotation in mid-surface, respectively.

<sup>158</sup> Subsequently, plugging Eqs. (1) and (5) into Eq. (4) and neglecting the  
<sup>159</sup> quadratic terms, the strain components can be rephrased as follows:

$$\begin{aligned} \epsilon_{\alpha\beta} &= \frac{1}{2}(\mathbf{a}_\alpha \cdot \mathbf{v}_{,\beta} + \mathbf{v}_{,\alpha} \cdot \mathbf{a}_\beta) \\ &+ \frac{1}{2}(\mathbf{a}_{3,\alpha} \cdot \mathbf{v}_{,\beta} + \mathbf{v}_{,\alpha} \cdot \mathbf{a}_{3,\beta} + \mathbf{a}_\alpha \cdot \boldsymbol{\theta}_{,\beta} + \boldsymbol{\theta}_{,\alpha} \cdot \mathbf{a}_\beta)\xi^3 \end{aligned} \quad (6a)$$

$$\epsilon_{\alpha 3} = \frac{1}{2}(\mathbf{a}_\alpha \cdot \boldsymbol{\theta} + \mathbf{v}_{,\alpha} \cdot \mathbf{a}_3) + \frac{1}{2}(\mathbf{a}_3 \cdot \boldsymbol{\theta})_{,\alpha}\xi^3 \quad (6b)$$

$$\epsilon_{33} = \mathbf{a}_3 \cdot \boldsymbol{\theta} \quad (6c)$$

<sup>160</sup> where  $\epsilon_{\alpha\beta}, \kappa_{\alpha\beta}$  represent membrane and bending strains, respectively, and are  
<sup>161</sup> given as follows:

$$\epsilon_{\alpha\beta} = \frac{1}{2}(\mathbf{a}_\alpha \cdot \mathbf{v}_{,\beta} + \mathbf{v}_{,\alpha} \cdot \mathbf{a}_\beta) \quad (7)$$

$$\kappa_{\alpha\beta} = \frac{1}{2}(\mathbf{a}_{3,\alpha} \cdot \mathbf{v}_{,\beta} + \mathbf{v}_{,\alpha} \cdot \mathbf{a}_{3,\beta} + \mathbf{a}_\alpha \cdot \boldsymbol{\theta}_{,\beta} + \boldsymbol{\theta}_{,\alpha} \cdot \mathbf{a}_\beta) \quad (8)$$

<sup>162</sup> In accordance with the Kirchhoff hypothesis, the thickness of shell will not  
<sup>163</sup> change, and the deformation related with direction of  $\xi^3$  will vanish, i.e.  $\epsilon_{3i} = 0$ .  
<sup>164</sup> Thus, the rotation  $\boldsymbol{\theta}$  can be rewritten as:

$$\epsilon_{3i} = 0 \Rightarrow \begin{cases} \boldsymbol{\theta} \cdot \mathbf{a}_\alpha = -\mathbf{v}_{,\alpha} \cdot \mathbf{a}_3 \\ \boldsymbol{\theta} \cdot \mathbf{a}_3 = 0 \end{cases} \Rightarrow \boldsymbol{\theta} = -\mathbf{v}_{,\alpha} \cdot \mathbf{a}_3 \mathbf{a}^\alpha \quad (9)$$

<sup>165</sup> where  $\mathbf{a}^\alpha$ 's is the in-plane contravariant base vector,  $\mathbf{a}^\alpha \cdot \mathbf{a}_\beta = \delta_\beta^\alpha$ ,  $\delta$  is the  
<sup>166</sup> Kronecker delta function. The detailed derivation of Eq. 9 can be found in [37].

<sup>167</sup> Furthermore, on substituting Eq. (9) into Eq. (8) leads to:

$$\kappa_{\alpha\beta} = (\Gamma_{\alpha\beta}^\gamma \mathbf{v}_{,\gamma} - \mathbf{v}_{,\alpha\beta}) \cdot \mathbf{a}_3 = -\mathbf{v}_{,\alpha}|_\beta \cdot \mathbf{a}_3 \quad (10)$$

<sup>168</sup> in which  $\Gamma_{\alpha\beta}^\gamma = \mathbf{a}_{\alpha,\beta} \cdot \mathbf{a}^\gamma$  is namely the Christoffel symbol of the second kind,  
<sup>169</sup> and  $\mathbf{v}_{,\alpha}|_\beta$  is the in-plane covariant derivative of  $\mathbf{v}_{,\alpha}$ , i.e.  $\mathbf{v}_{,\alpha}|_\beta = \Gamma_{\alpha\beta}^\gamma \mathbf{v}_{,\gamma} - \mathbf{v}_{,\alpha\beta}$ .

## <sup>170</sup> 2.2. Galerkin weak form for Hu-Washizu principle of complementary energy

<sup>171</sup> In this study, the Hu-Washizu variational principle of complementary energy  
<sup>172</sup> [38] was adopted for the development of the proposed analytical approach, the

<sup>174</sup> corresponding complementary functional, denoted by  $\Pi_C$ , is listed as follows:

$$\begin{aligned} & \Pi_C(\varepsilon_{\alpha\beta}, \kappa_{\alpha\beta}, N^{\alpha\beta}, M^{\alpha\beta}) \\ &= \int_{\Omega} \frac{h}{2} \varepsilon_{\alpha\beta} C^{\alpha\beta\gamma\eta} \varepsilon_{\gamma\eta} d\Omega + \int_{\Omega} \frac{h^3}{24} \kappa_{\alpha\beta} C^{\alpha\beta\gamma\eta} \kappa_{\gamma\eta} d\Omega \\ &+ \int_{\Omega} \varepsilon_{\alpha\beta} (N^{\alpha\beta} - h C^{\alpha\beta\gamma\eta} \varepsilon_{\gamma\eta}) d\Omega + \int_{\Omega} \kappa_{\alpha\beta} (M^{\alpha\beta} - \frac{h^3}{12} C^{\alpha\beta\gamma\eta} \kappa_{\gamma\eta}) d\Omega \\ &- \int_{\Gamma_v} \mathbf{T} \cdot \bar{\mathbf{v}} d\Gamma + \int_{\Gamma_\theta} M_{\mathbf{n}\mathbf{n}} \bar{\theta}_{\mathbf{n}} d\Gamma - (P \mathbf{a}_3 \cdot \bar{\mathbf{v}})_{\mathbf{x} \in C_w} \end{aligned} \quad (11)$$

<sup>175</sup> where  $C^{\alpha\beta\gamma\eta}$ 's represent the components of fourth order elasticity tensor with  
<sup>176</sup> respect to the covariant base and plane stress assumption, and it can be ex-  
<sup>177</sup> pressed by Young's modulus  $E$ , Poisson's ratio  $\nu$  and the in-plane contravariant  
<sup>178</sup> metric coefficients  $a^{\alpha\beta}$ 's,  $a^{\alpha\beta} = \mathbf{a}^\alpha \cdot \mathbf{a}^\beta$ , as follows:

$$C^{\alpha\beta\gamma\eta} = \frac{E}{2(1+\nu)} (a^{\alpha\gamma} a^{\beta\eta} + a^{\alpha\eta} a^{\beta\gamma} + \frac{2\nu}{1-\nu} a^{\alpha\beta} a^{\gamma\eta}) \quad (12)$$

<sup>179</sup> and  $N^{\alpha\beta}$ ,  $M^{\alpha\beta}$  represent the components of membrane- and bending- stresses  
<sup>180</sup> which are given by:

$$N^{\alpha\beta} = h C^{\alpha\beta\gamma\eta} \varepsilon_{\gamma\eta}, \quad M^{\alpha\beta} = \frac{h^3}{12} C^{\alpha\beta\gamma\eta} \kappa_{\gamma\eta} \quad (13)$$

<sup>181</sup> Essential boundaries on the edges and corners denoted by  $\Gamma_v$ ,  $\Gamma_\theta$  and  $C_v$   
<sup>182</sup> are naturally existed in complementary energy functional, and  $\bar{\mathbf{v}}$ ,  $\bar{\theta}_{\mathbf{n}}$  are the  
<sup>183</sup> corresponding prescribed displacement and normal rotation, respectively.  $\mathbf{T}$ ,  
<sup>184</sup>  $M_{\mathbf{n}\mathbf{n}}$  and  $P$  can be determined by Euler-Lagrange equations of shell problem  
<sup>185</sup> [37] as follows:

$$\mathbf{T} = \mathbf{T}_N + \mathbf{T}_M \rightarrow \begin{cases} \mathbf{T}_N = \mathbf{a}_\alpha N^{\alpha\beta} n_\beta \\ \mathbf{T}_M = (\mathbf{a}_3 M^{\alpha\beta} s_\alpha n_\beta)_{,\gamma} s^\gamma + (\mathbf{a}_3 M^{\alpha\beta})|_\beta n_\alpha \end{cases} \quad (14)$$

<sup>186</sup>  $M_{\mathbf{n}\mathbf{n}} = M^{\alpha\beta} n_\alpha n_\beta \quad (15)$

<sup>187</sup>  $P = -[[M^{\alpha\beta} s_\alpha n_\beta]] \quad (16)$

<sup>188</sup> where  $\mathbf{n} = n^\alpha \mathbf{a}_\alpha = n_\alpha \mathbf{a}^\alpha$  and  $\mathbf{s} = s^\alpha \mathbf{a}_\alpha = s_\alpha \mathbf{a}^\alpha$  are the outward normal and  
<sup>189</sup> tangent directions on boundaries.  $[[f]]$  is the jump operator defined by:

$$[[f]]_{\mathbf{x}=\mathbf{x}_c} = \lim_{\epsilon \rightarrow \mathbf{0}^+} (f(\mathbf{x}_c + \epsilon) - f(\mathbf{x}_c - \epsilon)), \mathbf{x}_c \in \Gamma \quad (17)$$

<sup>190</sup> where  $f$  is an arbitrary function on  $\Gamma$ .

<sup>191</sup> Moreover, the natural boundary conditions should be applied by Lagrangian  
<sup>192</sup> multiplier method with displacement  $\mathbf{v}$  regarded as multiplier. Thus, then the

<sup>193</sup> new complementary energy functional namely  $\Pi$  is given by:

$$\begin{aligned} & \Pi(\mathbf{v}, \varepsilon_{\alpha\beta}, \kappa_{\alpha\beta}, N^{\alpha\beta}, M^{\alpha\beta}) \\ &= \Pi_C(\varepsilon_{\alpha\beta}, \kappa_{\alpha\beta}, N^{\alpha\beta}, M^{\alpha\beta}) + \int_{\Gamma_M} \theta_n(M_{nn} - \bar{M}_{nn}) d\Gamma \\ & \quad - \int_{\Gamma_T} \mathbf{v} \cdot (\bar{\mathbf{T}}) d\Gamma - \mathbf{v} \cdot \mathbf{a}_3(P - \bar{P})_{x \in C_P} - \int_{\Omega} \mathbf{v} \cdot (\bar{\mathbf{b}}) d\Omega \end{aligned} \quad (18)$$

<sup>194</sup> where  $\bar{\mathbf{T}}$ ,  $\bar{M}_{nn}$  and  $\bar{P}$  are the prescribed traction, bending moment and con-  
<sup>195</sup> centrated force on edges  $\Gamma_T$ ,  $\Gamma_M$  and corner  $C_P$  respectively. All the specified  
<sup>196</sup> boundaries meet the following geometric relationships:

$$\begin{cases} \Gamma = \Gamma_v \cup \Gamma_T \cup \Gamma_\theta \cup \Gamma_M, & C = C_v \cup C_P, \\ \Gamma_v \cap \Gamma_T = \Gamma_\theta \cap \Gamma_M = C_v \cap C_P = \emptyset \end{cases} \quad (19)$$

<sup>197</sup> and  $\bar{\mathbf{b}}$  stands for the prescribed body force in  $\Omega$ ,  $\mathbf{b}$  can be written based on  
<sup>198</sup> Euler-Lagrange equations [37] as:

$$\mathbf{b} = \mathbf{b}_N + \mathbf{b}_M \rightarrow \begin{cases} \mathbf{b}_N = (\mathbf{a}_\alpha N^{\alpha\beta})|_\beta \\ \mathbf{b}_M = (\mathbf{a}_3 M^{\alpha\beta})|_{\alpha\beta} \end{cases} \quad (20)$$

<sup>199</sup> Introducing a standard variational argument to Eq. (18),  $\delta\Pi = 0$ , and  
<sup>200</sup> considering the arbitrariness of virtual variables,  $\delta\mathbf{v}$ ,  $\delta\varepsilon_{\alpha\beta}$ ,  $\delta\kappa_{\alpha\beta}$ ,  $N^{\alpha\beta}$ ,  $M^{\alpha\beta}$   
<sup>201</sup> lead to the following weak form:

$$-\int_{\Omega} h \delta\varepsilon_{\alpha\beta} C^{\alpha\beta\gamma\eta} \varepsilon_{\gamma\eta} d\Omega + \int_{\Omega} \delta\varepsilon_{\alpha\beta} N^{\alpha\beta} d\Omega = 0 \quad (21a)$$

$$-\int_{\Omega} \frac{h^3}{12} \delta\kappa_{\alpha\beta} C^{\alpha\beta\gamma\eta} \kappa_{\gamma\eta} d\Omega + \int_{\Omega} \delta\kappa_{\alpha\beta} M^{\alpha\beta} d\Omega = 0 \quad (21b)$$

$$\begin{aligned} \int_{\Omega} \delta N^{\alpha\beta} \varepsilon_{\alpha\beta} d\Omega - \int_{\Gamma} \delta \mathbf{T}_N \cdot \mathbf{v} d\Gamma + \int_{\Omega} \delta \mathbf{b}_N \cdot \mathbf{v} d\Omega \\ + \int_{\Gamma_v} \delta \mathbf{T}_N \cdot \mathbf{v} d\Gamma = \int_{\Gamma_v} \delta \mathbf{T}_N \cdot \bar{\mathbf{v}} d\Gamma \end{aligned} \quad (21c)$$

$$\begin{aligned} \int_{\Omega} \delta M^{\alpha\beta} \kappa_{\alpha\beta} d\Omega - \int_{\Gamma} \delta M_{nn} \theta_n d\Gamma + \int_{\Gamma} \delta \mathbf{T}_M \cdot \mathbf{v} d\Gamma + (\delta P \mathbf{a}_3 \cdot \mathbf{v})_{x \in C} + \int_{\Omega} \delta \mathbf{b}_M \cdot \mathbf{v} d\Omega \\ + \int_{\Gamma_\theta} \delta M_{nn} \theta_n d\Gamma - \int_{\Gamma_v} \delta \mathbf{T}_M \cdot \mathbf{v} d\Gamma - (\delta P \mathbf{a}_3 \cdot \mathbf{v})_{x \in C_v} \\ = \int_{\Gamma_\theta} \delta M_{nn} \bar{\theta}_n d\Gamma - \int_{\Gamma_v} \delta \mathbf{T}_M \cdot \bar{\mathbf{v}} d\Gamma - (\delta P \mathbf{a}_3 \cdot \bar{\mathbf{v}})_{x \in C_v} \end{aligned} \quad (21d)$$

<sup>205</sup>

$$\begin{aligned}
& \int_{\Gamma} \delta \theta_n M_{nn} d\Gamma - \int_{\Gamma} \delta \mathbf{v} \cdot \mathbf{T} d\Gamma - (\delta \mathbf{v} \cdot \mathbf{a}_3 P)_{x \in C} + \int_{\Omega} \delta \mathbf{v} \cdot \mathbf{b} d\Omega \\
& - \int_{\Gamma_\theta} \delta \theta_n M_{nn} d\Gamma + \int_{\Gamma_v} \delta \mathbf{v} \cdot \mathbf{T} d\Gamma + (\delta \mathbf{v} \cdot \mathbf{a}_3 P)_{x \in C_v} = - \int_{\Gamma_T} \delta \mathbf{v} \cdot \bar{\mathbf{t}} d\Gamma - \int_{\Omega} \delta \mathbf{v} \cdot \bar{\mathbf{b}} d\Omega
\end{aligned} \tag{21e}$$

<sup>206</sup> where the geometric relationships of Eq. (19) is used herein.

207    **3. Mixed meshfree formulation for modified Hu-Washizu's weak form**

208    *3.1. Reproducing kernel approximation for displacement*

209    This study approximates the displacement by adopting reproducing kernel  
 210    approximation. As shown in Fig. 2, the mid-surface of the shell  $\Omega$  is discretized  
 211    by a set of meshfree nodes  $\{\xi_I\}_{I=1}^{n_p}$  in parametric configuration, where  $n_p$  is the  
 212    total number of meshfree nodes. The approximated displacement namely  $\mathbf{v}^h$   
 213    can be expressed as:

$$\mathbf{v}(\xi) = \sum_{I=1}^{n_p} \Psi_I(\xi) \mathbf{d}_I \quad (22)$$

214    where  $\Psi_I$  and  $\mathbf{d}_I$  represent the shape function and nodal coefficient tensor re-  
 215    lated by node  $\xi_I$ . According to reproducing kernel approximation [18], the shape  
 216    function takes the following form:

$$\Psi_I(\xi) = \mathbf{p}^T(\xi) \mathbf{c}(\xi) \phi(\xi_I - \xi) \quad (23)$$

217    where  $\mathbf{p}$  is the basis function vector represented using the following quadratic  
 218    function as:

$$\mathbf{p} = \{1, \xi^1, \xi^2, (\xi^1)^2, \xi^1 \xi^2, (\xi^2)^2\}^T \quad (24)$$

219    The kernel function denoted by  $\phi$  controls the support and smoothness of  
 220    meshfree shape functions. The quintic B-spline function with square support is  
 221    used herein as the kernel function:

$$\phi(\xi_I - \xi) = \phi(\hat{s}_1) \phi(\hat{s}_2), \quad \hat{s}_\alpha = \frac{|\xi_I^\alpha - \xi^\alpha|}{s_{\alpha I}} \quad (25)$$

222    with

$$\phi(\hat{s}_\alpha) = \frac{1}{5!} \begin{cases} (3 - 3\hat{s}_\alpha)^5 - 6(2 - 3\hat{s}_\alpha)^5 + 15(1 - 3\hat{s}_\alpha)^5 & \hat{s}_\alpha \leq \frac{1}{3} \\ (3 - 3\hat{s}_\alpha)^5 - 6(2 - 3\hat{s}_\alpha)^5 & \frac{1}{3} < \hat{s}_\alpha \leq \frac{2}{3} \\ (3 - 3\hat{s}_\alpha)^5 & \frac{2}{3} < \hat{s}_\alpha \leq 1 \\ 0 & \hat{s}_\alpha > 1 \end{cases} \quad (26)$$

223    and  $s_{\alpha I}$  means the support size of meshfree shape function  $\Psi_I$ .

224    The unknown vector  $\mathbf{c}$  in shape function are determined by the fulfillment  
 225    of the so-called consistency condition:

$$\sum_{I=1}^{n_p} \Psi_I(\xi) \mathbf{p}(\xi_I) = \mathbf{p}(\xi) \quad (27)$$

226    or equivalently

$$\sum_{I=1}^{n_p} \Psi_I(\xi) \mathbf{p}(\xi_I - \xi) = \mathbf{p}(\mathbf{0}) \quad (28)$$

227    Substituting Eq. (22) into (28), yields:

$$\mathbf{A}(\xi) \mathbf{c}(\xi) = \mathbf{p}(\mathbf{0}) \Rightarrow \mathbf{c}(\xi) = \mathbf{A}^{-1}(\xi) \mathbf{p}(\mathbf{0}) \quad (29)$$

<sup>228</sup> where  $\mathbf{A}$  is the moment matrix:

$$\mathbf{A}(\xi) = \sum_{I=1}^{n_p} \phi(\xi_I - \xi) \mathbf{p}(\xi_I - \xi) \mathbf{p}^T(\xi_I - \xi) \quad (30)$$

<sup>229</sup> Substituting Eq. (29) back into Eq. (22), the expression of meshfree shape  
<sup>230</sup> function can be written as:

$$\Psi_I(\xi) = \mathbf{p}^T(\xi_I - \xi) \mathbf{A}^{-1}(\xi) \mathbf{p}(0) \phi(\xi_I - \xi) \quad (31)$$

<sup>231</sup> 3.2. Reproducing kernel gradient smoothing approximation for effective stress  
<sup>232</sup> and strain

<sup>233</sup> In Galerkin meshfree formulation, the mid-plane of thin shell  $\Omega$  is split by  
<sup>234</sup> a set of integration cells  $\Omega_C$ 's,  $\cup_{C=1}^{n_e} \Omega_C \approx \Omega$ , as shown in Fig. 2. With the  
<sup>235</sup> inspiration of reproducing kernel smoothing framework, the Cartesian and co-  
<sup>236</sup> variant derivatives of displacement,  $\mathbf{v}_{,\alpha}$  and  $-\mathbf{v}_{,\alpha}|_\beta$ , in strains  $\varepsilon_{\alpha\beta}$ ,  $\kappa_{\alpha\beta}$  are  
<sup>237</sup> approximated by  $(p-1)$ -th order polynomials in each integration cells. In inte-  
<sup>238</sup> gration cell  $\Omega_C$ , the approximated derivatives and strains denoted by  $\mathbf{v}_{,\alpha}^h$ ,  $\varepsilon_{\alpha\beta}^h$   
<sup>239</sup> and  $-\mathbf{v}_{,\alpha}^h|_\beta$ ,  $\kappa_{\alpha\beta}^h$  can be expressed by:

$$\mathbf{v}_{,\alpha}^h(\xi) = \mathbf{q}^T(\xi) \mathbf{d}_\alpha^\varepsilon, \quad \varepsilon_{\alpha\beta}^h(\xi) = \mathbf{q}^T(\xi) \frac{1}{2} (\mathbf{a}_\alpha \cdot \mathbf{d}_\beta^\varepsilon + \mathbf{a}_\beta \cdot \mathbf{d}_\alpha^\varepsilon) \quad (32)$$

$$-\mathbf{v}_{,\alpha}^h|_\beta(\xi) = \mathbf{q}^T(\xi) \mathbf{d}_{\alpha\beta}^\kappa, \quad \kappa_{\alpha\beta}^h(\xi) = \mathbf{q}^T(\xi) \mathbf{a}_3 \cdot \mathbf{d}_{\alpha\beta}^\kappa \quad (33)$$

<sup>241</sup> where  $\mathbf{q}$  is the linear polynomial vector and has the following form:

$$\mathbf{q} = \{1, \xi^1, \xi^2\} \quad (34)$$

<sup>242</sup> and the  $\mathbf{d}_\alpha^\varepsilon$ ,  $\mathbf{d}_{\alpha\beta}^\kappa$  are the corresponding coefficient vector tensors. For the con-  
<sup>243</sup> ciseness, the mixed usage of tensor and vector is introduced in this study. For  
<sup>244</sup> instance, the component of coefficient tensor vector  $\mathbf{d}_{\alpha I}^\varepsilon$ ,  $\mathbf{d}_\alpha^\varepsilon = \{\mathbf{d}_{\alpha I}^\varepsilon\}$ , is a three  
<sup>245</sup> dimensional tensor,  $\dim \mathbf{d}_{\alpha I}^\varepsilon = \dim \mathbf{v}$ .

<sup>246</sup> To satisfy the integration constraint of thin shell problem, the approximated  
<sup>247</sup> stresses  $N^{\alpha\beta h}$ ,  $M^{\alpha\beta h}$  were assumed to have a comparable form to strains, and  
<sup>248</sup> yields:

$$N^{\alpha\beta h}(\xi) = \mathbf{q}^T(\xi) \mathbf{a}^\alpha \cdot \mathbf{d}_N^\beta, \quad \mathbf{a}_\alpha N^{\alpha\beta h}(\xi) = \mathbf{q}^T(\xi) \mathbf{d}_N^\beta \quad (35)$$

$$M^{\alpha\beta h}(\xi) = \mathbf{q}^T(\xi) \mathbf{a}_3 \cdot \mathbf{d}_M^{\alpha\beta}, \quad \mathbf{a}_3 M^{\alpha\beta h}(\xi) = \mathbf{q}^T(\xi) \mathbf{d}_M^{\alpha\beta} \quad (36)$$

<sup>250</sup> substituting the approximations of Eqs. (22), (32), (33), (35), (36) into Eqs.  
<sup>251</sup> (21c), (21d) can express  $\mathbf{d}_\beta^\varepsilon$  and  $\mathbf{d}_{\alpha\beta}^\kappa$  by  $\mathbf{d}$  as:

$$\mathbf{d}_\beta^\varepsilon = \mathbf{G}^{-1} \left( \sum_{I=1}^{n_p} (\tilde{\mathbf{g}}_{\beta I} - \bar{\mathbf{g}}_{\beta I}) \mathbf{d}_I + \hat{\mathbf{g}}_\beta \right) \quad (37)$$

$$\mathbf{d}_{\alpha\beta}^\kappa = \mathbf{G}^{-1} \left( \sum_{I=1}^{n_p} (\tilde{\mathbf{g}}_{\alpha\beta I} - \bar{\mathbf{g}}_{\alpha\beta I}) \mathbf{d}_I + \hat{\mathbf{g}}_{\alpha\beta} \right) \quad (38)$$

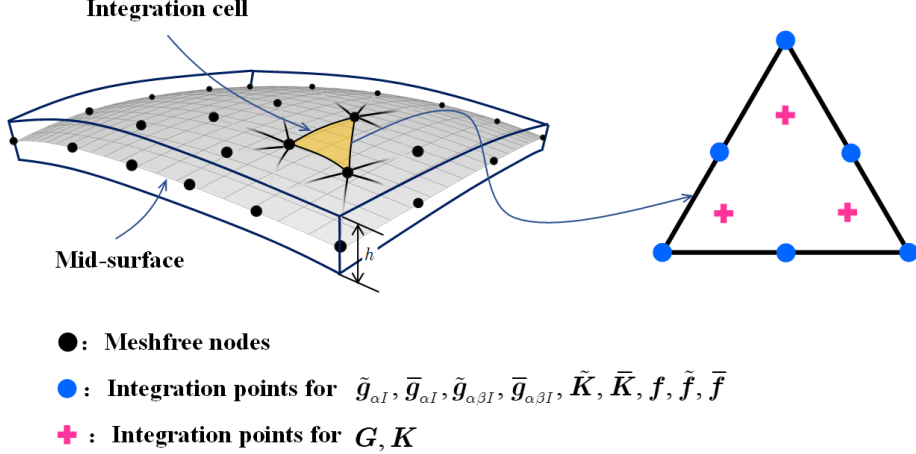


Figure 2: Integration scheme for Hu-Washizu weak form.

253 with

$$G = \int_{\Omega_C} \mathbf{q}^T \mathbf{q} d\Omega \quad (39)$$

254

$$\tilde{\mathbf{g}}_{\beta I} = \int_{\Gamma_C} \Psi_I \mathbf{q} n_{\beta} d\Gamma - \int_{\Omega_C} \Psi_I \mathbf{q}_{|\beta} d\Omega \quad (40a)$$

$$\bar{\mathbf{g}}_{\beta I} = \int_{\Gamma_C \cap \Gamma_v} \Psi_I \mathbf{q} n_{\beta} d\Gamma \quad (40b)$$

$$\hat{\mathbf{g}}_{\beta} = \int_{\Gamma_C \cap \Gamma_v} \mathbf{q} n_{\beta} \bar{\mathbf{v}} d\Gamma \quad (40c)$$

255

$$\begin{aligned} \tilde{\mathbf{g}}_{\alpha\beta I} &= \int_{\Gamma_C} \Psi_{I,\gamma} n^{\gamma} \mathbf{q} n_{\alpha} n_{\beta} d\Gamma - \int_{\Gamma_C} \Psi_I (\mathbf{q}_{|\beta} n_{\alpha} + (\mathbf{q} s_{\alpha} n_{\beta}),_{\gamma} s^{\gamma}) d\Gamma \\ &\quad + [[\Psi_I \mathbf{q} s_{\alpha} n_{\beta}]]_{x \in C_C} - \int_{\Omega_C} \Psi \mathbf{q}_{,\alpha|\beta} d\Omega \end{aligned} \quad (41a)$$

$$\begin{aligned} \bar{\mathbf{g}}_{\alpha\beta I} &= \int_{\Gamma_C \cap \Gamma_v} \Psi_{I,\gamma} n^{\gamma} \mathbf{q} n_{\alpha} n_{\beta} d\Gamma - \int_{\Gamma_C \cap \Gamma_v} \Psi_I (\mathbf{q}_{|\beta} n_{\alpha} + (\mathbf{q} s_{\alpha} n_{\beta}),_{\gamma} s^{\gamma}) d\Gamma \\ &\quad + [[\Psi_I \mathbf{q} s_{\alpha} n_{\beta}]]_{x \in C_C \cap C_v} \end{aligned} \quad (41b)$$

$$\begin{aligned} \hat{\mathbf{g}}_{\alpha\beta} &= \int_{\Gamma_C \cap \Gamma_v} \mathbf{q} n_{\alpha} n_{\beta} \mathbf{a}_3 \bar{\mathbf{n}} d\Gamma - \int_{\Gamma_C \cap \Gamma_v} (\mathbf{q}_{|\beta} n_{\alpha} + (\mathbf{q} s_{\alpha} n_{\beta}),_{\gamma} s^{\gamma}) \bar{\mathbf{v}} d\Gamma \\ &\quad + [[\mathbf{q} s_{\alpha} n_{\beta} \bar{\mathbf{v}}]]_{x \in C_C \cap C_v} \end{aligned} \quad (41c)$$

256 where evaluations of  $\mathbf{q}_{|\beta}$ ,  $\mathbf{q}_{,\alpha|\beta}$  are discussed in Appendix A. Further plugging  
257 Eqs. (37) and (38) back into Eqs. (32) and (33) respectively gives the final

<sup>258</sup> expression of  $\mathbf{v}_{,\alpha}^h$ ,  $\varepsilon_{\alpha\beta}^h$  and  $-\mathbf{v}_{,\alpha}^h|_\beta$ ,  $\kappa_{\alpha\beta}^h$  as:

$$\mathbf{v}_{,\alpha}^h = \sum_{I=1}^{n_p} (\tilde{\Psi}_{I,\alpha} - \bar{\Psi}_{I,\alpha}) \mathbf{d}_I + \mathbf{q}^T \mathbf{G}^{-1} \hat{\mathbf{g}}_\alpha \quad (42a)$$

$$\begin{aligned} \varepsilon_{\alpha\beta}^h &= \sum_{I=1}^{n_p} \frac{1}{2} (\mathbf{a}_\alpha \tilde{\Psi}_{I,\beta} + \mathbf{a}_\beta \tilde{\Psi}_{I,\alpha}) \cdot \mathbf{d}_I - \sum_{I=1}^{n_p} \frac{1}{2} (\mathbf{a}_\alpha \bar{\Psi}_{I,\beta} + \mathbf{a}_\beta \bar{\Psi}_{I,\alpha}) \cdot \mathbf{d}_I \\ &\quad + \mathbf{q}^T \mathbf{G}^{-1} \frac{1}{2} (\mathbf{a}_\alpha \cdot \hat{\mathbf{g}}_\beta + \mathbf{a}_\beta \cdot \hat{\mathbf{g}}_\alpha) \\ &= \tilde{\varepsilon}_{\alpha\beta}^h - \bar{\varepsilon}_{\alpha\beta}^h + \hat{\varepsilon}_{\alpha\beta}^h \end{aligned} \quad (42b)$$

$$-\mathbf{v}_{,\alpha}^h|_\beta = \sum_{I=1}^{n_p} (\tilde{\Psi}_{I,\alpha\beta} - \bar{\Psi}_{I,\alpha\beta}) \mathbf{d}_I + \mathbf{q}^T \mathbf{G}^{-1} \hat{\mathbf{g}}_{\alpha\beta} \quad (43a)$$

$$\begin{aligned} \kappa_{\alpha\beta}^h &= \sum_{I=1}^{n_p} \tilde{\Psi}_{I,\alpha\beta} \mathbf{a}_3 \cdot \mathbf{d}_I - \sum_{I=1}^{n_p} \bar{\Psi}_{I,\alpha\beta} \mathbf{a}_3 \cdot \mathbf{d}_I + \mathbf{q}^T \mathbf{G}^{-1} \mathbf{a}_3 \cdot \hat{\mathbf{g}}_{\alpha\beta} \\ &= \tilde{\kappa}_{\alpha\beta}^h - \bar{\kappa}_{\alpha\beta}^h + \hat{\kappa}_{\alpha\beta}^h \end{aligned} \quad (43b)$$

<sup>262</sup> with

$$\begin{cases} \tilde{\varepsilon}_{\alpha\beta}^h = \sum_{I=1}^{n_p} \frac{1}{2} (\mathbf{a}_\alpha \tilde{\Psi}_{I,\beta} + \mathbf{a}_\beta \tilde{\Psi}_{I,\alpha}) \cdot \mathbf{d}_I = \sum_{I=1}^{n_p} \tilde{\varepsilon}_{\alpha\beta I} \cdot \mathbf{d}_I \\ \bar{\varepsilon}_{\alpha\beta}^h = \sum_{I=1}^{n_p} \frac{1}{2} (\mathbf{a}_\alpha \bar{\Psi}_{I,\beta} + \mathbf{a}_\beta \bar{\Psi}_{I,\alpha}) \cdot \mathbf{d}_I = \sum_{I=1}^{n_p} \bar{\varepsilon}_{\alpha\beta I} \cdot \mathbf{d}_I \\ \hat{\varepsilon}_{\alpha\beta}^h = \mathbf{q}^T \mathbf{G}^{-1} \frac{1}{2} (\mathbf{a}_\alpha \cdot \hat{\mathbf{g}}_\beta + \mathbf{a}_\beta \cdot \hat{\mathbf{g}}_\alpha) \end{cases} \quad (44)$$

$$\begin{cases} \tilde{\Psi}_{I,\alpha}(\xi) = \mathbf{q}^T(\xi) \mathbf{G}^{-1} \tilde{\mathbf{g}}_{\alpha I} \\ \bar{\Psi}_{I,\alpha}(\xi) = \mathbf{q}^T(\xi) \mathbf{G}^{-1} \bar{\mathbf{g}}_{\alpha I} \\ \tilde{\varepsilon}_{\alpha\beta I} = \frac{1}{2} (\mathbf{a}_\alpha \tilde{\Psi}_{I,\beta} + \mathbf{a}_\beta \tilde{\Psi}_{I,\alpha}) \\ \bar{\varepsilon}_{\alpha\beta I} = \frac{1}{2} (\mathbf{a}_\alpha \bar{\Psi}_{I,\beta} + \mathbf{a}_\beta \bar{\Psi}_{I,\alpha}) \end{cases} \quad (45)$$

$$\begin{cases} \tilde{\kappa}_{\alpha\beta}^h = \sum_{I=1}^{n_p} \tilde{\Psi}_{I,\alpha\beta} \mathbf{a}_3 \cdot \mathbf{d}_I = \sum_{I=1}^{n_p} \tilde{\kappa}_{\alpha\beta I} \cdot \mathbf{d}_I \\ \bar{\kappa}_{\alpha\beta}^h = \sum_{I=1}^{n_p} \bar{\Psi}_{I,\alpha\beta} \mathbf{a}_3 \cdot \mathbf{d}_I = \sum_{I=1}^{n_p} \bar{\kappa}_{\alpha\beta I} \cdot \mathbf{d}_I \\ \hat{\kappa}_{\alpha\beta}^h = \mathbf{q}^T \mathbf{G}^{-1} \mathbf{a}_3 \cdot \hat{\mathbf{g}}_{\alpha\beta} \end{cases} \quad (46)$$

$$\begin{cases} \tilde{\Psi}_{I,\alpha\beta}(\xi) = \mathbf{q}^T(\xi) \mathbf{G}^{-1} \tilde{\mathbf{g}}_{\alpha\beta I} \\ \bar{\Psi}_{I,\alpha\beta}(\xi) = \mathbf{q}^T(\xi) \mathbf{G}^{-1} \bar{\mathbf{g}}_{\alpha\beta I} \\ \tilde{\kappa}_{\alpha\beta I} = \tilde{\Psi}_{I,\alpha\beta} \mathbf{a}_3 \\ \bar{\kappa}_{\alpha\beta I} = \bar{\Psi}_{I,\alpha\beta} \mathbf{a}_3 \end{cases} \quad (47)$$

266 It has to be noted that, referring to reproducing kernel gradient smoothing  
267 framework [33],  $\tilde{\Psi}_{I,\alpha}$ ,  $\tilde{\Psi}_{I,\alpha\beta}$  are actually the first and second order smoothed  
268 gradients in curvilinear coordinates. If the right hand side integration constraints  
269 for first and second order gradients are  $\tilde{\mathbf{g}}_{\alpha I}$  and  $\tilde{\mathbf{g}}_{\alpha\beta I}$ , respectively, then this for-  
270 mulation can satisfy the variational consistency for the second order polynomi-  
271 als. It should be mentioned that in curved model, the variational consistency for  
272 non-polynomial functions, such as trigonometric functions, should be required  
273 for the polynomial solution. Even with high order polynomial variational consis-  
274 tency, the proposed formulation cannot exactly reproduce the solution spanned  
275 by the basis functions. However, the accuracy of reproducing kernel smoothed  
276 gradients is still superior than the traditional meshfree formulation. The nu-  
277 mercial examples in the following section will better demonstrate the precision  
278 of the reproducing kernel smoothed gradients.

279    **4. Naturally variational enforcement for essential boundary condi-**  
 280    **tions**

281    *4.1. Discrete equilibrium equations*

282    With the approximated effective stresses and strains, the last equation of  
 283    weak form Eq. (21e) becomes:

$$-\sum_{C=1}^{n_e} \sum_{I=1}^{n_p} \delta \mathbf{d}_I \cdot \left( (\tilde{\mathbf{g}}_{\alpha I}^T - \bar{\mathbf{g}}_{\alpha I}^T) \mathbf{d}_N^\alpha + (\tilde{\mathbf{g}}_{\alpha\beta I}^T - \bar{\mathbf{g}}_{\alpha\beta I}^T) \mathbf{d}_M^{\alpha\beta} \right) = -\sum_{I=1}^{n_p} \delta \mathbf{d}_I \cdot \mathbf{f}_I \quad (48)$$

284    where  $\mathbf{f}_I$ 's denote the components of the traditional force vector:

$$\mathbf{f}_I = \int_{\Gamma_t} \Psi_I \bar{\mathbf{t}} d\Gamma - \int_{\Gamma_M} \Psi_{I,\gamma} n^\gamma \bar{M}_{\mathbf{n}\mathbf{n}} d\Gamma + [[\Psi_I \mathbf{a}_3 \bar{P}]]_{\mathbf{x} \in C_P} + \int_{\Omega} \Psi_I \bar{\mathbf{b}} d\Omega \quad (49)$$

285    The left side of Eq. (48) can be simplified using the following steps. For clarity,  
 286    the derivation of first term in Eq. (48) taken as an example is given by:

$$\begin{aligned} \sum_{I=1}^{n_p} \delta \mathbf{d}_I \cdot \tilde{\mathbf{g}}_{\alpha I}^T \mathbf{d}_N^\alpha &= \sum_{I=1}^{n_p} \delta \mathbf{d}_I \cdot (\mathbf{G}^{-1} \tilde{\mathbf{g}}_{\alpha I})^T \mathbf{G} \mathbf{d}_N^\alpha \\ &= \int_{\Omega_C} \sum_{I=1}^{n_p} \delta \mathbf{d}_I \cdot (\mathbf{q}^T \mathbf{G}^{-1} \tilde{\mathbf{g}}_{\alpha I}) \mathbf{q}^T \mathbf{d}_N^\alpha d\Omega \\ &= \int_{\Omega_C} \sum_{I=1}^{n_p} \delta \mathbf{d}_I \cdot \mathbf{a}_\beta (\mathbf{q}^T \mathbf{G}^{-1} \tilde{\mathbf{g}}_{\alpha I}) N^{\alpha\beta h} d\Omega \\ &= \int_{\Omega_C} \delta \tilde{\varepsilon}_{\alpha\beta}^h N^{\alpha\beta h} d\Omega \end{aligned} \quad (50)$$

<sup>287</sup> following the above procedure and including the weak form of Eqs. (21a), (21b),  
<sup>288</sup> the left side of Eq. (48) in  $\Omega_C$  becomes:

$$\begin{aligned}
& \sum_{I=1}^{n_p} \delta \mathbf{d}_I \cdot \left( (\tilde{\mathbf{g}}_{\alpha I}^T - \bar{\mathbf{g}}_{\alpha I}^T) \mathbf{d}_N^\alpha + (\tilde{\mathbf{g}}_{\alpha \beta I}^T - \bar{\mathbf{g}}_{\alpha \beta I}^T) \mathbf{d}_M^{\alpha \beta} \right) \\
& = \int_{\Omega_C} ((\delta \tilde{\varepsilon}_{\alpha \beta}^h - \delta \bar{\varepsilon}_{\alpha \beta}^h) N^{\alpha \beta h} + (\delta \tilde{\kappa}_{\alpha \beta}^h - \delta \bar{\kappa}_{\alpha \beta}^h) M^{\alpha \beta h}) d\Omega \\
& = \int_{\Omega_C} (\delta \tilde{\varepsilon}_{\alpha \beta}^h - \delta \bar{\varepsilon}_{\alpha \beta}^h) h C^{\alpha \beta \gamma \eta} \varepsilon_{\gamma \eta}^h + (\delta \tilde{\kappa}_{\alpha \beta}^h - \delta \bar{\kappa}_{\alpha \beta}^h) \frac{h^3}{12} C^{\alpha \beta \gamma \eta} \kappa_{\gamma \eta}^h \\
& = \int_{\Omega_C} \delta \tilde{\varepsilon}_{\alpha \beta}^h h C^{\alpha \beta \gamma \eta} \tilde{\varepsilon}_{\gamma \eta}^h d\Omega + \int_{\Omega_C} \delta \tilde{\kappa}_{\alpha \beta}^h \frac{h^3}{12} C^{\alpha \beta \gamma \eta} \tilde{\kappa}_{\gamma \eta}^h d\Omega \\
& - \int_{\Omega_C} \delta \bar{\varepsilon}_{\alpha \beta}^h h C^{\alpha \beta \gamma \eta} \bar{\varepsilon}_{\gamma \eta}^h d\Omega - \int_{\Omega_C} \delta \bar{\varepsilon}_{\alpha \beta}^h h C^{\alpha \beta \gamma \eta} \tilde{\varepsilon}_{\gamma \eta}^h d\Omega \\
& - \int_{\Omega_C} \delta \tilde{\kappa}_{\alpha \beta}^h \frac{h^3}{12} C^{\alpha \beta \gamma \eta} \bar{\kappa}_{\gamma \eta}^h d\Omega - \int_{\Omega_C} \delta \bar{\kappa}_{\alpha \beta}^h \frac{h^3}{12} C^{\alpha \beta \gamma \eta} \tilde{\kappa}_{\gamma \eta}^h d\Omega \\
& + \int_{\Omega_C} \delta \bar{\varepsilon}_{\alpha \beta}^h h C^{\alpha \beta \gamma \eta} \bar{\varepsilon}_{\gamma \eta}^h d\Omega + \int_{\Omega_C} \delta \bar{\kappa}_{\alpha \beta}^h \frac{h^3}{12} C^{\alpha \beta \gamma \eta} \bar{\kappa}_{\gamma \eta}^h d\Omega \\
& + \int_{\Omega_C} (\delta \tilde{\varepsilon}_{\alpha \beta}^h - \delta \bar{\varepsilon}_{\alpha \beta}^h) h C^{\alpha \beta \gamma \eta} \tilde{\varepsilon}_{\gamma \eta}^h d\Omega + \int_{\Omega_C} (\delta \tilde{\kappa}_{\alpha \beta}^h - \delta \bar{\kappa}_{\alpha \beta}^h) \frac{h^3}{12} C^{\alpha \beta \gamma \eta} \tilde{\kappa}_{\gamma \eta}^h d\Omega
\end{aligned} \tag{51}$$

<sup>289</sup> The complete discrete equilibrium equations can be obtained by further substituting  
<sup>290</sup> Eqs. (44) and (46) into above equation, respectively:

$$(\mathbf{K} + \tilde{\mathbf{K}} + \bar{\mathbf{K}}) \mathbf{d} = \mathbf{f} + \tilde{\mathbf{f}} + \bar{\mathbf{f}} \tag{52}$$

<sup>291</sup> where the components of stiffness matrices and force vectors in discrete equilibrium  
<sup>292</sup> equations can be evaluated as follows:

$$\mathbf{K}_{IJ} = \int_{\Omega} \tilde{\varepsilon}_{\alpha \beta I} h C^{\alpha \beta \gamma \eta} \tilde{\varepsilon}_{\gamma \eta J} d\Omega + \int_{\Omega} \tilde{\kappa}_{\alpha \beta I} \frac{h^3}{12} C^{\alpha \beta \gamma \eta} \tilde{\kappa}_{\gamma \eta J} d\Omega \tag{53}$$

<sup>293</sup>

$$\begin{aligned}
\tilde{\mathbf{K}}_{IJ} & = - \int_{\Gamma_v} (\Psi_I \tilde{\mathbf{T}}_{NJ} + \tilde{\mathbf{T}}_{NI} \Psi_J) d\Gamma \\
& + \int_{\Gamma_\theta} (\Psi_{I,\gamma} n^\gamma \mathbf{a}_3 \tilde{\mathbf{M}}_{nnJ} + \mathbf{a}_3 \tilde{\mathbf{M}}_{nnI} \Psi_{J,\gamma} n^\gamma) d\Gamma \\
& + ([[\Psi_I \mathbf{a}_3 \tilde{\mathbf{P}}_J]] + [[\tilde{\mathbf{P}}_I \mathbf{a}_3 \Psi_J]])_{\mathbf{x} \in C_v}
\end{aligned} \tag{54a}$$

$$\tilde{\mathbf{f}}_I = - \int_{\Gamma_v} \tilde{\mathbf{T}}_{NI} \cdot \bar{\mathbf{v}} d\Gamma + \int_{\Gamma_\theta} \tilde{\mathbf{M}}_{nnI} \bar{\theta}_n d\Gamma + [[\tilde{\mathbf{P}}_I \mathbf{a}_3 \cdot \bar{\mathbf{v}}]]_{\mathbf{x} \in C_v} \tag{54b}$$

<sup>294</sup>

$$\bar{\mathbf{K}}_{IJ} = - \int_{\Gamma_v} \bar{\mathbf{T}}_{MI} \Psi_J d\Gamma + \int_{\Gamma_\theta} \mathbf{a}_3 \bar{\mathbf{M}}_{nnI} \Psi_{J,\gamma} n^\gamma d\Gamma + [[\bar{\mathbf{P}}_I \mathbf{a}_3 \Psi_J]]_{\mathbf{x} \in C_v} \tag{55a}$$

$$\bar{\mathbf{f}}_I = - \int_{\Gamma_v} \bar{\mathbf{T}}_{MI} \cdot \bar{\mathbf{v}} d\Gamma + \int_{\Gamma_\theta} \bar{\mathbf{M}}_{nnI} \bar{\theta}_n d\Gamma + [[\bar{\mathbf{P}}_I \mathbf{a}_3 \cdot \bar{\mathbf{v}}]]_{\mathbf{x} \in C_v} \tag{55b}$$

295 The detailed derivations of Eqs (53)-(55) are listed in the Appendix B. As  
 296 shown in these equations, Eq. (53) is the conventional stiffness matrix eval-  
 297 uated by smoothed gradients  $\tilde{\Psi}_{I,\alpha}$ ,  $\tilde{\Psi}_{I,\alpha}|_{\beta}$ , and the Eqs. (54) and (55) contribute  
 298 for the enforcement of essential boundary. It should be noticed that, in accord-  
 299 ance with reproducing kernel smoothed gradient framework, the integration  
 300 scheme of Eqs. (53-55) should be aligned with those used in the construction of  
 301 smoothed gradients. The integration scheme used for the proposed method is  
 302 shown in Fig. 2, in which the total number of the blue circular integration points  
 303 has been optimized from a global point of view, aiming to reduce the computa-  
 304 tion of traditional meshfree shape functions and its first order derivatives. In  
 305 contrast, for assembly stiffness matrix  $\mathbf{K}$ , the low order Gauss integration rule  
 306 is suitable to ensure the accuracy due to the inherently variational consistency  
 307 in the smoothed gradients. The detailed positions and weight of the integration  
 308 points and the efficiency demonstration of this optimized integration scheme  
 309 can be found in [33, 39]. Examining Eqs. (54) and (55), closely reveal that the  
 310 structure of the suggested approach to enforce essential boundary conditions is  
 311 identical to that of the conventional Nitsche's method, with both having the  
 312 consistent and stabilized terms. Thus, a review of Nitsche's method and a com-  
 313 parison with the proposed approach will be provided in the next subsection.

314 *4.2. Comparison with Nitsche's method*

315 The Nitsche's method for enforcing essential boundaries can be regarded as a  
 316 combination of Lagrangian multiplier method and penalty method, in which the  
 317 Lagrangian multiplier is represented by the approximated displacement. The  
 318 corresponding total potential energy functional  $\Pi_P$  is given by:

$$\begin{aligned}
 \Pi_P(\mathbf{v}) = & \int_{\Omega} \frac{1}{2} \varepsilon_{\alpha\beta} N^{\alpha\beta} d\Omega + \int_{\Omega} \frac{1}{2} \kappa_{\alpha\beta} M^{\alpha\beta} d\Omega \\
 & - \int_{\Gamma_t} \mathbf{v} \cdot \bar{\mathbf{t}} d\Gamma + \int_{\Gamma_M} \mathbf{v}_{,\gamma} n^{\gamma} \mathbf{a}_3 M_{\mathbf{n}\mathbf{n}} d\Gamma + (\mathbf{v} \cdot \mathbf{a}_3 P)_{\mathbf{x} \in C_P} - \int_{\Omega} \mathbf{v} \cdot \bar{\mathbf{b}} d\Omega \\
 & - \underbrace{\int_{\Gamma_v} \mathbf{t} \cdot (\mathbf{v} - \bar{\mathbf{v}}) d\Gamma + \int_{\Gamma_{\theta}} M_{\mathbf{n}\mathbf{n}} (\theta_{\mathbf{n}} - \bar{\theta}_{\mathbf{n}}) d\Gamma + (P \mathbf{a}_3 \cdot (\mathbf{v} - \bar{\mathbf{v}}))_{\mathbf{x} \in C_v}}_{\text{consistent term}} \quad (56) \\
 & + \underbrace{\sum_{i=1}^3 \frac{\alpha_{vi}}{2} \int_{\Gamma_v} (\mathbf{v} \cdot \mathbf{a}_i)^2 d\Gamma + \frac{\alpha_{\theta}}{2} \int_{\Gamma_{\theta}} \theta_{\mathbf{n}}^2 d\Gamma + \frac{\alpha_C}{2} (\mathbf{v} \cdot \mathbf{a}_3)^2_{\mathbf{x} \in C_v}}_{\text{stabilized term}}
 \end{aligned}$$

319 where the consistent term generated from the Lagrangian multiplier method con-  
 320 tributes to enforce the essential boundary, and meet the variational consistency  
 321 condition. However, the consistent term can not always ensure the coercivity  
 322 of stiffness, so the penalty method is introduced to serve as a stabilized term,  
 323 in which  $\alpha_{vi}$  is the experimental artificial parameter to enforce the displace-  
 324 ment towards the  $\mathbf{a}_i$  direction,  $\alpha_{\theta}$  and  $\alpha_C$  are parameters to enforce rotation  
 325 and corner deflection, respectively. With a standard variational argument, the

<sup>326</sup> corresponding weak form can be stated as:

$$\begin{aligned}
\delta\Pi_P(\mathbf{v}) &= \int_{\Omega} \delta\varepsilon_{\alpha\beta} N^{\alpha\beta} d\Omega + \int_{\Omega} \delta\kappa_{\alpha\beta} M^{\alpha\beta} d\Omega \\
&\quad - \int_{\Gamma_t} \delta\mathbf{v} \cdot \bar{\mathbf{t}} d\Gamma + \int_{\Gamma_M} \delta\mathbf{v}_{,\gamma} n^\gamma \mathbf{a}_3 M_{\mathbf{n}\mathbf{n}} d\Gamma + (\delta\mathbf{v} \cdot \mathbf{a}_3 P)_{\mathbf{x} \in C_P} - \int_{\Omega} \delta\mathbf{v} \cdot \bar{\mathbf{b}} d\Omega \\
&\quad - \int_{\Gamma_v} \delta\mathbf{v} \cdot \mathbf{t} d\Gamma + \int_{\Gamma_\theta} \delta\theta_{\mathbf{n}} M_{\mathbf{n}\mathbf{n}} d\Gamma + (\mathbf{v} \cdot \mathbf{a}_3 P)_{\mathbf{x} \in C_v} \\
&\quad - \int_{\Gamma_v} \delta\mathbf{t} \cdot (\mathbf{v} - \bar{\mathbf{v}}) d\Gamma + \int_{\Gamma_\theta} \delta M_{\mathbf{n}\mathbf{n}} (\theta_{\mathbf{n}} - \bar{\theta}_{\mathbf{n}}) d\Gamma + (\delta P \mathbf{a}_3 \cdot (\mathbf{v} - \bar{\mathbf{v}}))_{\mathbf{x} \in C_v} \\
&\quad + \sum_{i=1}^3 \alpha_{vi} \int_{\Gamma_v} (\delta\mathbf{v} \cdot \mathbf{a}_i) (\mathbf{a}_i \cdot \mathbf{v}) d\Gamma + \alpha_\theta \int_{\Gamma_\theta} \delta\theta_{\mathbf{n}} \theta_{\mathbf{n}} d\Gamma + \alpha_C (\delta\mathbf{v} \cdot \mathbf{a}_3 \mathbf{a}_3 \cdot \mathbf{v})_{\mathbf{x} \in C_v} \\
&= 0
\end{aligned} \tag{57}$$

<sup>327</sup> Upon further invoking the conventional reproducing kernel approximation of  
<sup>328</sup> Eq. (22), the subsequent discrete equilibrium equations can be obtained:

$$(\mathbf{K} + \mathbf{K}^c + \mathbf{K}^s)\mathbf{d} = \mathbf{f} + \mathbf{f}^c + \mathbf{f}^s \tag{58}$$

<sup>329</sup> where the stiffness  $\mathbf{K}$  is identical with Eq. (53).  $\mathbf{K}^c$  and  $\mathbf{K}^s$  are the stiffness  
<sup>330</sup> matrices for consistent and stabilized terms, respectively, and their components  
<sup>331</sup> have the following form:

$$\begin{aligned}
\mathbf{K}_{IJ}^c &= - \int_{\Gamma_v} (\Psi_I \mathbf{T}_{NJ} + \mathbf{T}_{NI} \Psi_J) d\Gamma \\
&\quad + \int_{\Gamma_\theta} (\Psi_{I,\gamma} n^\gamma \mathbf{a}_3 \mathbf{M}_{\mathbf{n}\mathbf{n}J} + \mathbf{a}_3 \mathbf{M}_{\mathbf{n}\mathbf{n}I} \Psi_{J,\gamma} n^\gamma) d\Gamma \\
&\quad + ([[ \Psi_I \mathbf{a}_3 \mathbf{P}_J ]]] + [[ \mathbf{P}_I \mathbf{a}_3 \Psi_J ]])_{\mathbf{x} \in C_v}
\end{aligned} \tag{59a}$$

$$\mathbf{f}_I^c = - \int_{\Gamma_v} \mathbf{T}_I \cdot \bar{\mathbf{v}} d\Gamma + \int_{\Gamma_\theta} \mathbf{M}_{\mathbf{n}\mathbf{n}I} \bar{\theta}_{\mathbf{n}} d\Gamma + [[ \mathbf{P}_I \mathbf{a}_3 \cdot \bar{\mathbf{v}} ]]_{\mathbf{x} \in C_v} \tag{59b}$$

<sup>332</sup>

$$\mathbf{K}_{IJ}^s = \boldsymbol{\alpha}_v \int_{\Gamma_v} \Psi_I \Psi_J d\Gamma + \alpha_\theta \int_{\Gamma_\theta} \Psi_{I,\eta} n^\eta \mathbf{a}_3 \mathbf{a}_3 n^\gamma \Psi_{J,\gamma} d\Gamma + \alpha_C [[ \Psi_I \mathbf{a}_3 \mathbf{a}_3 \Psi_J ]]_{\mathbf{x} \in C_v} \tag{60a}$$

$$\mathbf{f}_I^s = \boldsymbol{\alpha}_v \int_{\Gamma_v} \Psi_I \bar{\mathbf{v}} d\Gamma + \alpha_\theta \int_{\Gamma_\theta} \Psi_{I,\eta} n^\eta \mathbf{a}_3 \bar{\theta}_{\mathbf{n}} d\Gamma + \alpha_C [[ \Psi_I \mathbf{a}_3 \mathbf{a}_3 \cdot \bar{\mathbf{v}} ]]_{\mathbf{x} \in C_v} \tag{60b}$$

<sup>333</sup> with

$$\boldsymbol{\alpha}_v = \begin{bmatrix} \alpha_{v1} & 0 & 0 \\ 0 & \alpha_{v2} & 0 \\ 0 & 0 & \alpha_{v3} \end{bmatrix} \tag{61}$$

<sup>334</sup> On comparing with the consistent terms of Eqs. (54) and (59), the ex-  
<sup>335</sup> pressions were almost identical, the major difference is that the higher order

<sup>336</sup> derivatives of shape functions have been replaced by the smoothed gradients.  
<sup>337</sup> Owing to the reproducing kernel framework, the construction of the smoothed  
<sup>338</sup> gradients only concerned about the computation of traditional meshfree shape  
<sup>339</sup> functions and their first order derivatives, which avoid the costly computation  
<sup>340</sup> of higher order derivatives. Moreover, the stabilized terms in Eq. (60) em-  
<sup>341</sup> ploys the penalty method with big enough artificial parameters to ensure the  
<sup>342</sup> coercivity of stiffness. Besides, the optimal values of these artificial parame-  
<sup>343</sup> ters are proportional to the grid size of discrete model that can be represented  
<sup>344</sup> by the support size in meshfree approximation, where  $\alpha_{v\alpha} \propto s^{-1}$ ,  $\alpha_{v3} \propto s^{-3}$ ,  
<sup>345</sup>  $\alpha_\theta \propto s^{-1}$ ,  $\alpha_C \propto s^{-2}$ [37], and  $s = \min\{s_{\alpha I}\}$ . In contrast, the stabilized term of  
<sup>346</sup> Eq. (55) naturally exists in its weak form, and can stabilize the result without  
<sup>347</sup> considering any artificial parameters.

348    **5. Numerical examples**

349    In this section, the suggested method is validated through several exam-  
 350    ples using the Nitsche's method, the consistent reproducing kernel gradient  
 351    smoothing integration scheme (RKGSI), and the non-consistent Gauss integra-  
 352    tion scheme (GI) with penalty method, as well as the proposed Hu-Washizu  
 353    formulation (HW) to enforce the necessary boundary conditions. A normalized  
 354    support size of 2.5 is used for all the considered methods to ensure the require-  
 355    ment of quadratic base meshfree approximation. To eliminate the influence of  
 356    integration error, the Gauss integration scheme uses 6 Gauss points for domain  
 357    integration and 3 points for boundary integration, so as to maintain the same  
 358    integration accuracy between domain and boundaries. Moreover, the number  
 359    of integration points are identical between the Gauss and RKGSI schemes. The  
 360    error estimates of displacement ( $L_2$ -Error) and energy ( $H_e$ -Error) is used here:

$$L_2\text{-Error} = \frac{\sqrt{\int_{\Omega}(\mathbf{v} - \mathbf{v}^h) \cdot (\mathbf{v} - \mathbf{v}^h) d\Omega}}{\sqrt{\mathbf{v} \cdot \mathbf{v}}}$$

$$H_e\text{-Error} = \frac{\sqrt{\int_{\Omega} \left( (\varepsilon_{\alpha\beta} - \varepsilon_{\alpha\beta}^h)(N^{\alpha\beta} - N^{\alpha\beta h}) + \int_{\Omega} (\kappa_{\alpha\beta} - \kappa_{\alpha\beta}^h)(M^{\alpha\beta} - M^{\alpha\beta h}) \right) d\Omega}}{\sqrt{\int_{\Omega} (\varepsilon_{\alpha\beta} N^{\alpha\beta} + \kappa_{\alpha\beta} M^{\alpha\beta}) d\Omega}}$$
(62)

361    *5.1. Patch tests*

362    The linear and quadratic patch tests for flat and curved thin shells are firstly  
 363    studied to verify the variational consistency of the proposed method. As shown  
 364    in Fig. 3, the flat and curved models are depicted by an identical parametric  
 365    domain  $\Omega = (0, 1) \otimes (0, 1)$ , where the cylindrical coordinate system with radius  
 366     $R = 1$ , thickness  ~~$h = 0.1$~~   $\underline{h = 0.05}$  is employed to describe the curved model,  
 367    and the whole domain  $\Omega$  is discretized by the 165 meshfree nodes. The Young's  
 368    modulus and Poisson's ratio of thin shell are set to  $E = 1$ ,  $\nu = 0$ . The artificial  
 369    parameters of  $\alpha_v = 10^5 \times E$ ,  $\alpha_\theta = 10^3 \times E$ ,  $\alpha_C = 10^5 \times E$  and  $\alpha_v = 10^9 \times$   
 370     $E$ ,  $\alpha_\theta = 10^9 \times E$ ,  $\alpha_C = 10^9 \times E$  were adopted in Nitsche's- and penalty- method,  
 371    respectively. All the boundaries are enforced as essential boundary conditions  
 372    with the following manufactured exact solution:

$$\mathbf{v} = \begin{cases} (\xi^1 + 2\xi^2)^n \\ (3\xi^1 + 4\xi^2)^n \\ (5\xi^1 + 6\xi^2)^n \end{cases}, \quad n = \begin{cases} 1 & \text{Linear patch test} \\ 2 & \text{Quadratic patch test} \end{cases}$$
(63)

373    Table 1 lists the  $L_2$ - and  $H_e$ -Error results of patch test with flat model, where  
 374    the RKGSI scheme with variational consistent essential boundary enforcement,  
 375    i.e. RKGSI-Nitsche and RKGSI-HW, can pass the linear and quadratic patch  
 376    test. In contrast, the RKGSI-Penalty cannot pass the patch test since the  
 377    Penalty method is unable to ensure the variational consistency. Due to the  
 378    loss of variational consistency condition, even with the Nitsche's method, Gauss

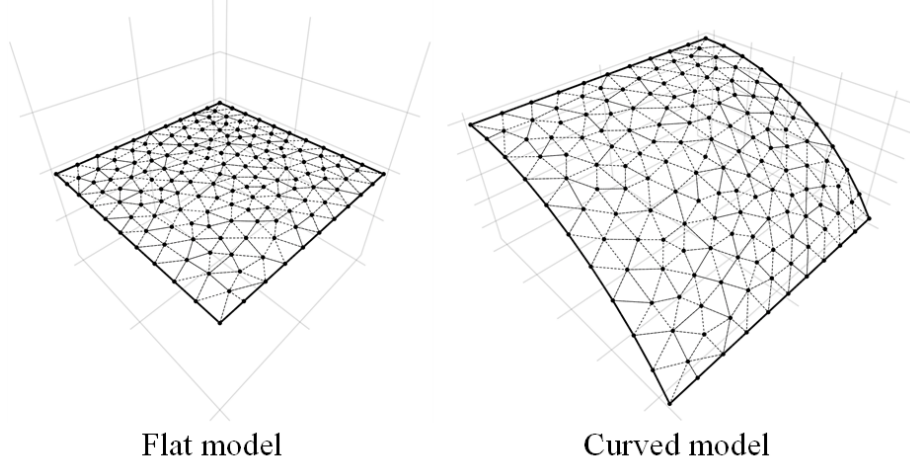


Figure 3: Meshfree discretization for patch test

meshfree formulations show noticeable errors. Table 2 shows the results for curved model, which indicated that all the considered methods cannot pass the patch test. This is mainly because the proposed smoothed gradient of Eqs. (35) and (36) could not exactly reproduce the non-polynomial membrane and bending stresses. On the other hand, the RKGSI-HW and RKGSI-Nitsche methods provide better accuracy compared to the other approaches due to the fulfillment of first second-order variational consistency. Even only with local variational consistency, the RKGSI-Penalty obtained a better result than the traditional Gauss scheme. Meanwhile, the bending moment contours of  $M^{12}$  are listed in Fig. 4, which further verify that the proposed method provided a satisfactory result compared to the exact solution. Contrarily, both the RKGSI-Penalty and the conventional Gauss meshfree formulations observed errors.

Table 1: Results of patch test for flat model.

	Linear patch test		Quadratic patch test	
	$L_2$ -Error	$H_e$ -Error	$L_2$ -Error	$H_e$ -Error
GI-Penalty	<u>4.451.41E-04</u>	<u>1.35E-02</u> <u>4.62E-03</u>	<u>2.041.97E-03</u>	<u>1.63E-02</u> <u>7.17E-03</u>
GI-Nitsche	<u>4.511.73E-04</u>	<u>1.42E-02</u> <u>5.61E-03</u>	<u>1.221.85E-03</u>	<u>1.68E-02</u> <u>7.76E-03</u>
RKGSI-Penalty	<u>3.645.04E-09</u>	<u>6.77E-08</u> <u>1.02E-07</u>	<u>4.543.01E-09</u>	<u>6.573.41E-08</u>
RKGSI-Nitsche	<u>3.319.75E-12</u>	<u>1.348.98E-11</u>	<u>5.981.29E-12</u>	<u>1.21E-11</u> <u>1.06E-12</u>
RKGSI-HR	<u>6.676.15E-13</u>	<u>1.50E-11</u> <u>1.076.91E-12</u>	<u>1.26E-11</u> <u>7.51E-13</u>	<u>8.36E-12</u>

### 5.2. Scordelis-Lo roof

This example considers the classical Scordelis-Lo roof problem, as depicted in Fig. 5. The cylindrical roof has dimensions  $R = 25$ ,  $L = 50$ ,  $h = 0.25$ ,

Table 2: Results of patch test for cylindrical model.

	Linear patch test		Quadratic patch test	
	$L_2$ -Error	$H_e$ -Error	$L_2$ -Error	$H_e$ -Error
GI-Penalty	3.791.75E-04	1.30E-02 4.50E-03	1.741.08E-03	1.37E-02 5.83E-03
GI-Nitsche	4.041.77E-04	1.42E-02 5.36E-03	1.151.07E-03	1.49E-02 6.33E-03
RKGSI-Penalty	1.478.59E-05	9.11E-04	5.39E-03 2.264.28E-04	2.092.08E-03
RKGSI-Nitsche	2.41E-06 1.27E-05	7.375.32E-05	2.47E-06 2.891.88E-05	5.6E-04
RKGSI-HR	4.28E-06 1.43E-05	1.301.60E-04	9.69E-06 2.93E-05	2.412.85E-04

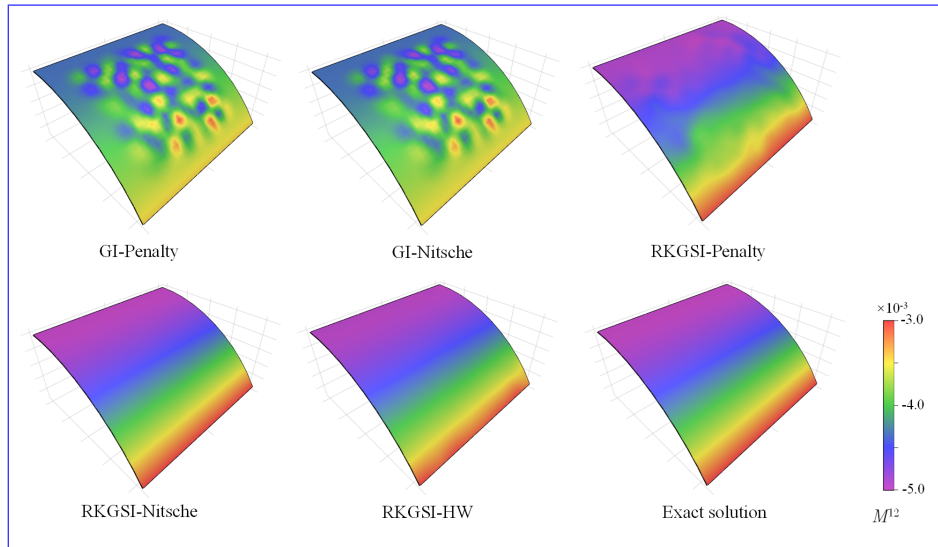


Figure 4: Contour plots of  $M^{12}$  for curved shell patch test.

394 Young's modulus  $E = 4.32 \times 10^8$  and Poisson's ratio  $\nu = 0.0$ . The entire roof  
395 is subjected to an uniform body force of  $b_z = -90$ , with the straight edges  
396 remaining free and the the curved edges are enforced by  $v_x = v_z = 0$ .

397 Due to the symmetry, only a quadrant of the model is considered for meshfree  
398 analysis, which is discretized by the  $11 \times 16$ ,  $13 \times 20$ ,  $17 \times 24$  and  $19 \times 28$  meshfree  
399 nodes, as listed in Fig. 6. The comparison of the displacement in  $z$ -direction  
400 at node  $A$ ,  $v_{A3}$ , is used as the investigated quantity, with the reference value  
401 0.3006 given by [9]. Firstly, Fig. 7 presents a sensitivity study for the artificial  
402 parameters of  $\alpha_{vi}$ 's and  $\alpha_\theta$ 's in the RKGSI meshfree formulations with the  
403 Nitsche's- and penalty- method, where all of the parameters are scaled by the  
404 support size as,  $\alpha_{v\alpha} = s^{-1}\bar{\alpha}_v$ ,  $\alpha_{v3} = s^{-3}\bar{\alpha}_v$  and  $\alpha_\theta = s^{-1}\bar{\alpha}_\theta$ . For a better  
405 comparison, the result of the proposed RKGSI-HW is also listed in this figure.  
406 The results of Fig. 7 revealed, that Nitsche's method observed less artificial  
407 sensitivity. However, both the methods cannot trivially determine the optimal  
408 values of the artificial parameters. The optimal artificial parameters from Fig.

<sup>409</sup> 7 are adopted for the convergence study in Fig. 8. The convergence result  
<sup>410</sup> showed that the RKGSI method get satisfactory results while the traditional  
<sup>411</sup> Gauss methods demonstrated noticeable errors.

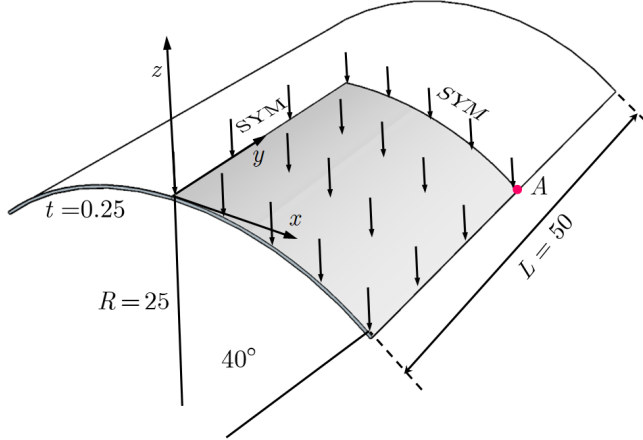


Figure 5: Description of Scordelis-Lo roof problem.

### <sup>412</sup> 5.3. Pinched Hemispherical shell

<sup>413</sup> Consider the hemispherical shell shown in Fig. 9, which is loaded at four  
<sup>414</sup> points  $P = \pm 2$  at  $90^\circ$  interval at its bottom. The hemispherical shell has an  
<sup>415</sup> radius  $R = 10$ , thickness  $h = 0.04$ , Young's modulus  $E = 6.825 \times 10^7$  and  
<sup>416</sup> Poisson's ratio  $\nu = 0.3$ .

<sup>417</sup> Due to symmetry, only quadrant model, where the  $16 \times 16$ ,  $24 \times 24$ ,  $32 \times 32$   
<sup>418</sup> and  $40 \times 40$  meshfree nodes have been discretized as shown in Fig. (10), were con-  
<sup>419</sup>sidered. The quantity under investigation for convergence is the displacement  
<sup>420</sup> at  $x$ -direction on point  $A$ ,  $v_{A1} = 0.094$  [40]. Fig. 11 displays the corresponding  
<sup>421</sup> convergence results, indicating the RKGSI scheme performed significantly better  
<sup>422</sup> compared to the GI meshfree formulation. Meanwhile, the efficiency comparison  
<sup>423</sup> for this problem is also shown in Fig. 12, in which the CPU time for assembly  
<sup>424</sup> and calculation of shape functions are considered. Fig. 12(a) indicates that the  
<sup>425</sup> RKGSI scheme observed high efficiency in assembly. This is due to the vari-  
<sup>426</sup>ational inconsistent Gauss meshfree formulation which require more Gaussian  
<sup>427</sup> points to get satisfactory results. Fig. 12(b) lists the CPU time spent on enforc-  
<sup>428</sup>ing essential boundary conditions for the penalty method, Nitsche's method and  
<sup>429</sup>proposed HW method. The results highlighted that the proposed HW method  
<sup>430</sup>consumed comparable CPU time in assembly compared to Nitsche's method.  
<sup>431</sup> However, less time was spent to calculate the shape functions. Since both the  
<sup>432</sup>HW method and penalty method were developed considering the shape func-  
<sup>433</sup>tions first order derivatives. For this reason, both the methods shared an almost  
<sup>434</sup>identical time in computing the shape functions.

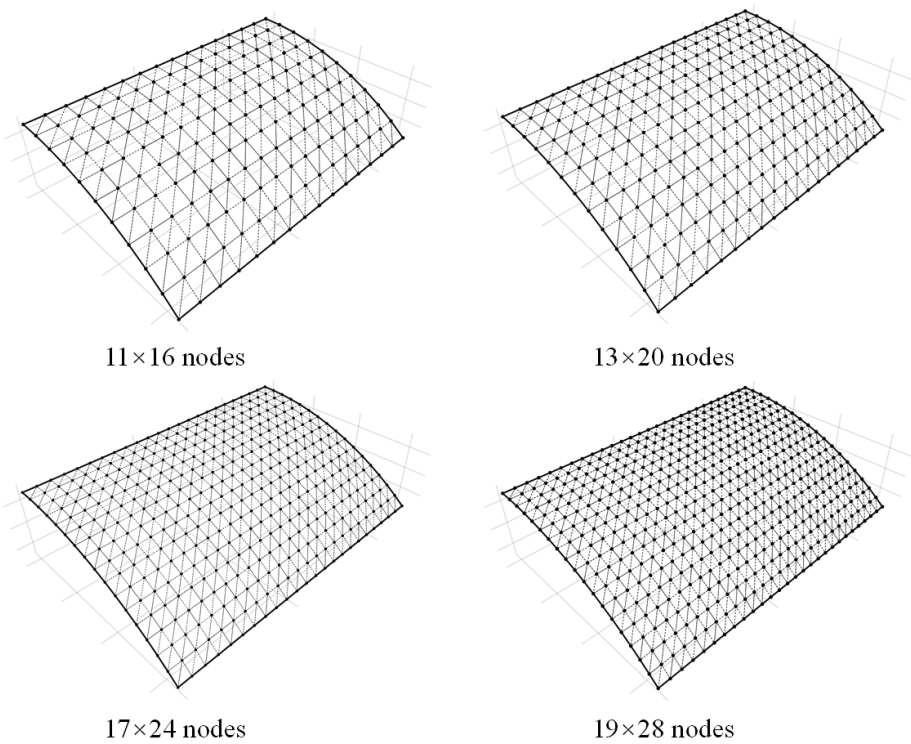
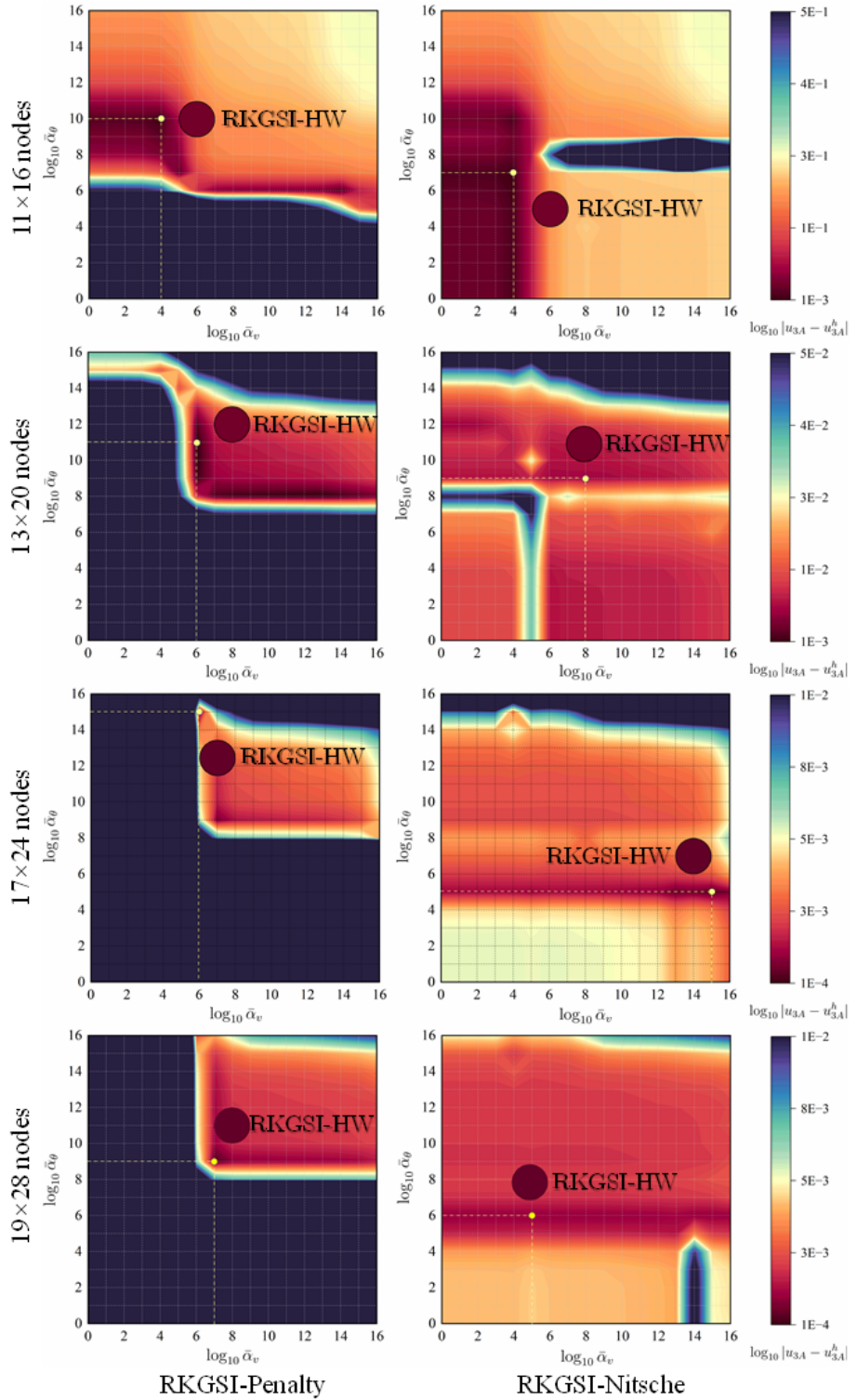


Figure 6: Meshfree discretizations for Scordelis-Lo roof problem.

Figure 7: Sensitivity comparison of  $\alpha_v$  and  $\alpha_\theta$  for Scordelis-Lo problem.

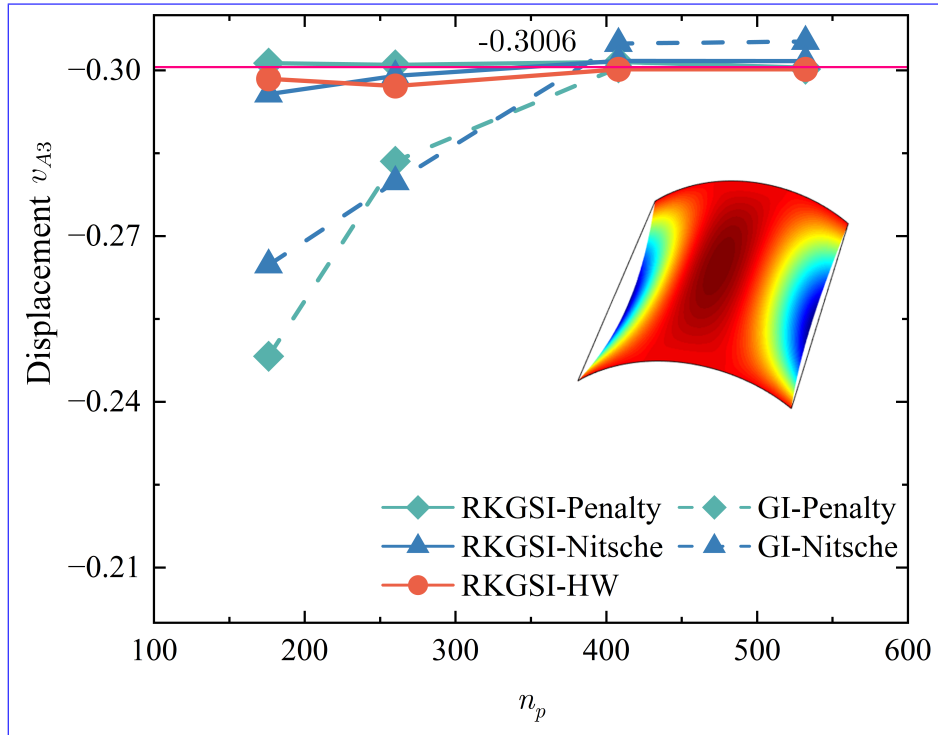


Figure 8: Displacement convergence for Scordelis-Lo roof problem.

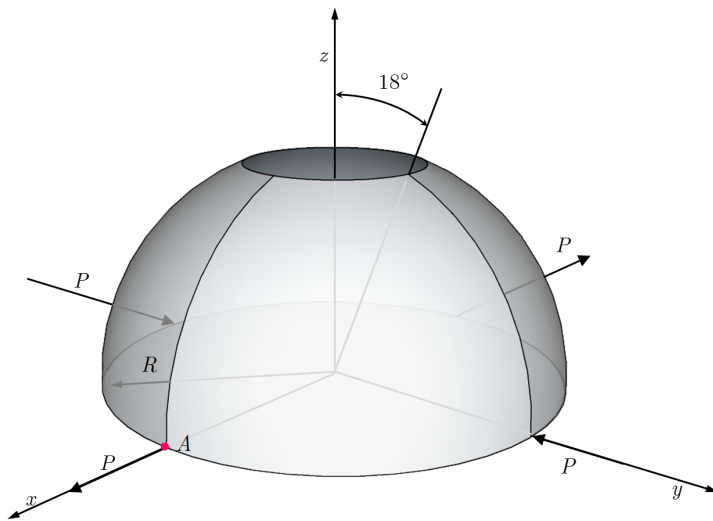


Figure 9: Description of pinched hemispherical shell problem.

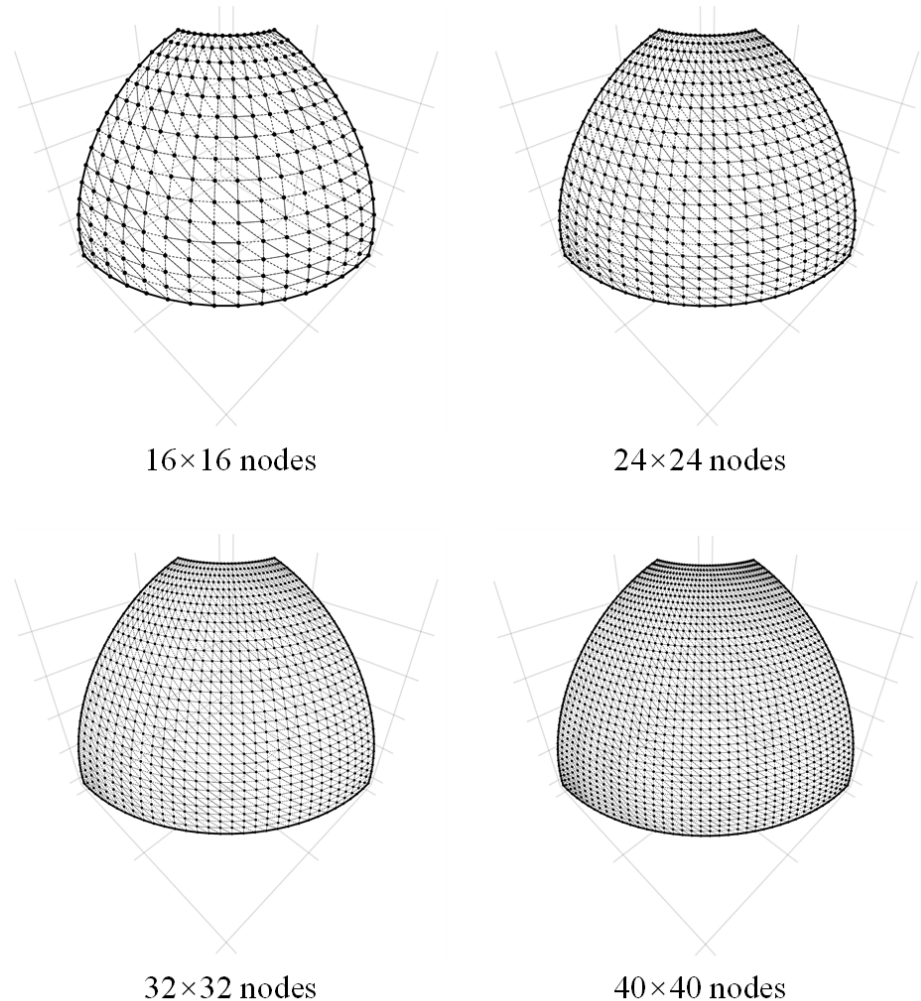


Figure 10: Meshfree discretizations for pinched hemispherical shell problem.

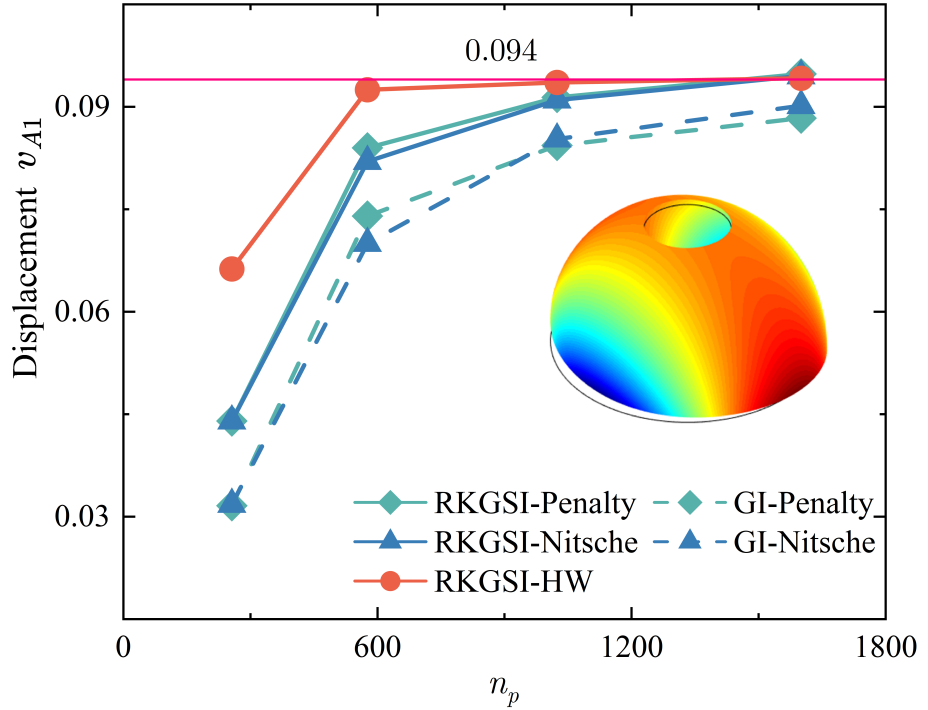


Figure 11: Displacement convergence for pinched hemispherical shell problem.

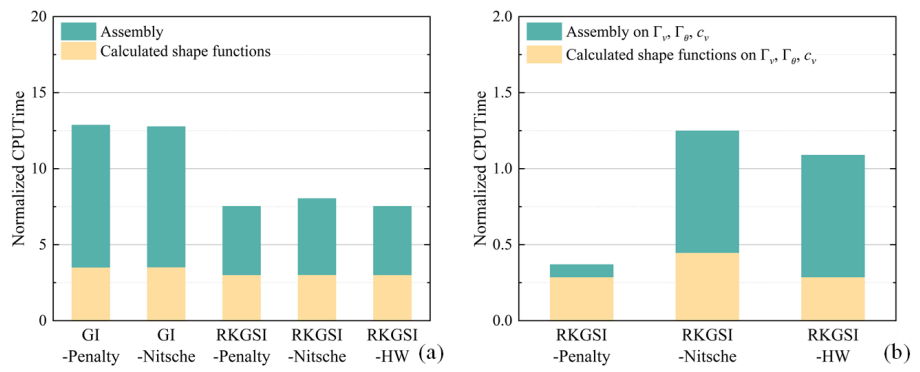


Figure 12: Efficiency comparison for pinched hemispherical shell problem: (a) Whole domain; (b) Essential boundaries

435     **6. Conclusion**

436     In this study, an efficient and quasi-consistent meshfree thin shell formu-  
437     lation was presented to naturally enforce the essential boundary conditions.  
438     Mixed formulation with the Hu-Washizu principle weak form is adopted, where  
439     the traditional meshfree shape functions discretized the displacement, and the  
440     strains and stresses were expressed by the reproducing kernel smoothed gra-  
441     dients and the covariant bases, respectively. The smoothed gradient naturally  
442     embedded the first second-order integration constraints and has a quasi varia-  
443     tional consistency for the curved models in each integration cell. Owing to the  
444     Hu-Washizu variational principle, the essential boundary condition enforcement  
445     has a similar form with the conventional Nitsche's method; both have consistent  
446     and stabilized terms. The costly high order derivatives in the Nitsche's consis-  
447     tent term have been replaced by the smoothed gradients, which improved the  
448     computational speed due to the reproducing kernel gradient smoothing frame-  
449     work. Furthermore, the stabilized term naturally existed in the Hu-Washizu  
450     weak form, and the artificial parameter needed in Nitsche's stabilized term has  
451     vanished, which can automatically maintain the coercivity for the stiffness ma-  
452     trix. Based on general reproducing kernel gradient smoothing framework, the  
453     proposed methodology can be trivially extended to high order basis meshfree for-  
454     mulation. The numerical results demonstrated that the proposed Hu-Washizu  
455     quasi-consistent meshfree thin shell formulation showed excellent accuracy, effi-  
456     ciency, and stability.

457      **Acknowledgment**

458      The support of this work by the National Natural Science Foundation of  
459      China (12102138, 52350410467) and the Natural Science Foundation of Fujian  
460      Province of China (2023J01108, 2022J05056) is gratefully acknowledged.

<sup>461</sup> **Appendix A. Green's theorems for in-plane vector**

<sup>462</sup> This Appendix discusses two kinds of Green's theorems used for the development  
<sup>463</sup> of the proposed meshfree method. For an arbitrary vectors  $v^\alpha$  and a  
<sup>464</sup> scalar function  $f$ , with Green's theorem for in-plane vector, the first Green's  
<sup>465</sup> theorem is listed as follows [37]:

$$\begin{aligned} \int_{\Omega} f_{,\alpha} v^\alpha d\Omega &= \int_{\Gamma} f v^\alpha n_\alpha d\Gamma - \int_{\Omega} f(v_{,\alpha}^\alpha + \Gamma_{\beta\alpha}^\beta v^\alpha) d\Omega \\ &= \int_{\Gamma} f v^\alpha n_\alpha d\Gamma - \int_{\Omega} f v^\alpha|_\alpha d\Omega \end{aligned} \quad (\text{A.1})$$

<sup>466</sup> where  $\Gamma_{\alpha\beta}^\gamma = \mathbf{a}_{\alpha,\beta} \cdot \mathbf{a}^\gamma$  denotes the Christoffel symbol of the second kind.  $v^\alpha|_\alpha$   
<sup>467</sup> can be represented as the in-plane covariant derivative of the vector  $v^\alpha$ :

$$v^\alpha|_\alpha = v_{,\alpha}^\alpha + \Gamma_{\beta\alpha}^\beta v^\alpha \quad (\text{A.2})$$

<sup>468</sup> The second Green's theorem is established with a mixed form of second  
<sup>469</sup> order derivative. Let  $A^{\alpha\beta}$  can be an arbitrary symmetric second order tensor,  
<sup>470</sup> the Green's theorem yields [37]:

$$\begin{aligned} \int_{\Omega} f_{,\alpha}|_\beta A^{\alpha\beta} d\Omega &= \int_{\Gamma} f_{,\gamma} n^\gamma A^{\alpha\beta} n_\alpha n_\beta d\Gamma - \int_{\Gamma} f(A^{\alpha\beta} s_\alpha n_\beta)_{,\gamma} s^\gamma d\Gamma + [[f A^{\alpha\beta} s_\alpha n_\beta]]_{\mathbf{x}\in C} \\ &\quad - \int_{\Gamma} f(A_{,\beta}^{\alpha\beta} n_\alpha + \Gamma_{\alpha\beta}^\gamma A^{\alpha\beta} n_\gamma + \Gamma_{\gamma\beta}^\gamma A^{\alpha\beta} n_\alpha) d\Gamma \\ &\quad + \int_{\Omega} f \left( \begin{array}{l} \Gamma_{\alpha\beta,\gamma}^\gamma A^{\alpha\beta} + \Gamma_{\alpha\beta}^\gamma A^{\alpha\beta} + \Gamma_{\eta\gamma}^\eta \Gamma_{\alpha\beta}^\gamma A^{\alpha\beta} \\ + A_{,\alpha\beta}^{\alpha\beta} + \Gamma_{\gamma\beta,\alpha}^\gamma A^{\alpha\beta} + 2\Gamma_{\gamma\alpha}^\gamma A_{,\beta}^{\alpha\beta} + \Gamma_{\gamma\alpha}^\gamma \Gamma_{\eta\beta}^\eta A^{\alpha\beta} \end{array} \right) d\Omega \\ &= \int_{\Gamma} f_{,\gamma} n^\gamma A^{\alpha\beta} n_\alpha n_\beta d\Gamma - \int_{\Gamma} f(A^{\alpha\beta} s_\alpha n_\beta)_{,\gamma} s^\gamma d\Gamma + [[f A^{\alpha\beta} s_\alpha n_\beta]]_{\mathbf{x}\in C} \\ &\quad - \int_{\Gamma} f A^{\alpha\beta}|_\beta n_\alpha d\Gamma + \int_{\Omega} f A^{\alpha\beta}|_\alpha n_\beta d\Omega \end{aligned} \quad (\text{A.3})$$

<sup>471</sup> with

$$A^{\alpha\beta}|_\beta = A_{,\beta}^{\alpha\beta} + \Gamma_{\beta\gamma}^\alpha A^{\beta\gamma} + \Gamma_{\gamma\beta}^\alpha A^{\alpha\beta} \quad (\text{A.4})$$

$$\begin{aligned} A^{\alpha\beta}|_{\alpha\beta} &= \Gamma_{\alpha\beta,\gamma}^\gamma A^{\alpha\beta} + \Gamma_{\alpha\beta}^\gamma A^{\alpha\beta} + \Gamma_{\eta\gamma}^\eta \Gamma_{\alpha\beta}^\gamma A^{\alpha\beta} \\ &\quad + A_{,\alpha\beta}^{\alpha\beta} + \Gamma_{\gamma\beta,\alpha}^\gamma A^{\alpha\beta} + 2\Gamma_{\gamma\alpha}^\gamma A_{,\beta}^{\alpha\beta} + \Gamma_{\gamma\alpha}^\gamma \Gamma_{\eta\beta}^\eta A^{\alpha\beta} \end{aligned} \quad (\text{A.5})$$

<sup>473</sup> For the sake of brevity, the notion of covariant derivative is extended to a  
<sup>474</sup> scalar function as:

$$f|_\alpha = f_{,\alpha} + \Gamma_{\beta\alpha}^\beta f \quad (\text{A.6})$$

$$f|_\beta n_\alpha = f_{,\beta} n_\alpha + \Gamma_{\alpha\beta}^\gamma f n_\gamma + \Gamma_{\gamma\beta}^\gamma f n_\alpha \quad (\text{A.7})$$

$$\begin{aligned} f|_{\alpha\beta} &= \Gamma_{\alpha\beta,\gamma}^\gamma f + \Gamma_{\alpha\beta}^\gamma f_{,\gamma} + \Gamma_{\eta\gamma}^\eta \Gamma_{\alpha\beta}^\gamma f \\ &\quad + f_{,\alpha\beta} + \Gamma_{\gamma\beta,\alpha}^\gamma f + 2\Gamma_{\gamma\alpha}^\gamma f_{,\beta} + \Gamma_{\gamma\alpha}^\gamma \Gamma_{\eta\beta}^\eta f \end{aligned} \quad (\text{A.8})$$

<sup>477</sup> **Appendix B. Derivations for stiffness metrics and force vectors**

<sup>478</sup> This Appendix details the derivations of stiffness matrices and force vectors  
<sup>479</sup> in Eqs. (53)-(55), where the relationships of Eqs. (40), (41), (44) and (46) are  
<sup>480</sup> used herein. Firstly, the membrane strain terms are considered as follows:

$$\begin{aligned}
 & \sum_{C=1}^{n_e} \int_{\Omega_C} \delta \tilde{\varepsilon}_{\alpha\beta}^h h C^{\alpha\beta\gamma\eta} \tilde{\varepsilon}_{\gamma\eta}^h d\Omega \\
 &= \sum_{C=1}^{n_e} \sum_{I,J=1}^{n_p} \delta \mathbf{d}_I \cdot \underbrace{\int_{\Omega_C} \tilde{\varepsilon}_{\alpha\beta I} h C^{\alpha\beta\gamma\eta} \mathbf{a}_\gamma \mathbf{q}^T d\Omega \mathbf{G}^{-1} \bar{\mathbf{g}}_{\eta J} \cdot \mathbf{d}_J}_{\tilde{\mathbf{g}}_I^{\eta T}} \\
 &= \sum_{C=1}^{n_e} \sum_{I,J=1}^{n_p} \delta \mathbf{d}_I \cdot \underbrace{\int_{\Gamma_C \cap \Gamma_v} \Psi_J \mathbf{q}^T \mathbf{G}^{-1} \tilde{\mathbf{g}}_I^\alpha n_\alpha d\Gamma}_{\tilde{\mathbf{T}}_{NI}} \cdot \mathbf{d}_J \\
 &= \sum_{I,J=1}^{n_p} \delta \mathbf{d}_I \cdot \int_{\Gamma_v} \tilde{\mathbf{T}}_{NI} \Psi_J d\Gamma \cdot \mathbf{d}_J
 \end{aligned} \tag{B.1}$$

<sup>481</sup> with

$$\tilde{\mathbf{g}}_I^\alpha = \mathbf{q} \mathbf{a}_\beta h C^{\alpha\beta\gamma\eta} \tilde{\varepsilon}_{\gamma\eta I} \tag{B.2}$$

$$\tilde{\mathbf{T}}_{NI} = \mathbf{q}^T \mathbf{G}^{-1} \tilde{\mathbf{g}}_I^\alpha n_\alpha \tag{B.3}$$

<sup>483</sup> Following this path, the bending strain terms can be reorganized by:

$$\begin{aligned}
 & \sum_{C=1}^{n_e} \int_{\Omega_C} \delta \tilde{\kappa}_{\alpha\beta}^h \frac{h^3}{12} C^{\alpha\beta\gamma\eta} \tilde{\kappa}_{\gamma\eta}^h d\Omega \\
 &= \sum_{C=1}^{n_e} \sum_{I,J=1}^{n_p} \delta \mathbf{d}_I \cdot \underbrace{\int_{\Omega_C} \tilde{\kappa}_{\alpha\beta I} \frac{h^3}{12} C^{\alpha\beta\gamma\eta} \mathbf{a}_3 \mathbf{q}^T d\Omega \mathbf{G}^{-1} \bar{\mathbf{g}}_{\gamma\eta J} \cdot \mathbf{d}_J}_{\tilde{\mathbf{g}}_I^{\gamma\eta T}} \\
 &= \sum_{C=1}^{n_e} \sum_{I,J=1}^{n_p} \delta \mathbf{d}_I \cdot \left( \begin{array}{l} \int_{\Gamma_C \cap \Gamma_\theta} \underbrace{\mathbf{q}^T \mathbf{G}^{-1} \tilde{\mathbf{g}}_I^{\alpha\beta} n_\alpha n_\beta}_{\tilde{\mathbf{M}}_{nnI}} n^\gamma \Psi_{J,\gamma} d\Gamma \\ - \int_{\Gamma_C \cap \Gamma_v} \underbrace{(\mathbf{q}_{\beta}^T \mathbf{G}^{-1} \tilde{\mathbf{g}}_I^{\alpha\beta} n_\alpha + (\mathbf{q}^T \mathbf{G}^{-1} \tilde{\mathbf{g}}_I^{\alpha\beta} s_\alpha n_\beta)_{,\gamma} s^\gamma)}_{\tilde{\mathbf{T}}_{MI}} \Psi_J d\Gamma \\ + [[\underbrace{\mathbf{q}^T \mathbf{G}^{-1} \tilde{\mathbf{g}}_I^{\alpha\beta} s_\alpha n_\beta}_{\tilde{\mathbf{P}}_I \mathbf{a}_3} \Psi_J]]_{\mathbf{x} \in C_C \cap C_v} \end{array} \right) \cdot \mathbf{d}_J \\
 &= \sum_{I,J=1}^{n_p} \delta \mathbf{d}_I \cdot \left( \int_{\Gamma_\theta} \tilde{\mathbf{M}}_{nnI} n^\gamma \Psi_{J,\gamma} d\Gamma - \int_{\Gamma_v} \tilde{\mathbf{T}}_{MI} \Psi_J d\Gamma + [[\tilde{\mathbf{P}}_I \Psi_J]]_{\mathbf{x} \in C_v} \right)
 \end{aligned} \tag{B.4}$$

<sup>484</sup> with

$$\tilde{\mathbf{g}}_I^{\alpha\beta} = \int_{\Omega_C} \mathbf{q} \frac{h^3}{12} C^{\alpha\beta\gamma\eta} \mathbf{a}_3 \tilde{\boldsymbol{\kappa}}_{\gamma\eta I} d\Omega \quad (\text{B.5})$$

<sup>485</sup>

$$\begin{cases} \tilde{M}_{nnI} = \mathbf{q}^T \mathbf{G}^{-1} \tilde{\mathbf{g}}_I^{\alpha\beta} n_\alpha n_\beta \\ \tilde{T}_{MI} = \mathbf{q}_{|\beta}^T \mathbf{G}^{-1} \tilde{\mathbf{g}}_I^{\alpha\beta} n_\alpha + (\mathbf{q}^T \mathbf{G}^{-1} \tilde{\mathbf{g}}_I^{\alpha\beta} s_\alpha n_\beta)_{,\gamma} s^\gamma \\ \tilde{P}_I = \mathbf{q}^T \mathbf{G}^{-1} \tilde{\mathbf{g}}_I^{\alpha\beta} s_\alpha n_\beta \cdot \mathbf{a}_3 \end{cases} \quad (\text{B.6})$$

486      **References**

- 487      [1] L. H. Donnell, Beams, Plates and Shells, McGraw-Hill, 1976.
- 488      [2] S. Ahmad, B. M. Irons, O. C. Zienkiewicz, Analysis of thick and thin shell  
489      structures by curved finite elements, International Journal for Numerical  
490      Methods in Engineering 2 (1970) 419–451.
- 491      [3] T. J. Hughes, The Finite Element Method: Linear Static and Dynamic  
492      Finite Element Analysis, Dover Publications, Mineola, New York, 2000.  
493      T. Belytschko, Y. Y. Lu, L. Gu, Element-free Galerkin methods,  
494      International Journal for Numerical Methods in Engineering 37 (1994)  
495      229–256.
- 496      [4] J. C. Simo, D. D. Fox, On a stress resultant geometrically exact shell model.  
497      Part I: Formulation and optimal parametrization, Computer Methods in  
498      Applied Mechanics and Engineering 72 (1989) 267–304.  
499      W. K. Liu, S. Jun, Y. F. Zhang, Reproducing kernel particle methods,  
500      International Journal for Numerical Methods in Fluids 20 (1995)  
501      1081–1106.
- 502      [5] P. Krysl, T. Belytschko, Analysis of thin shells by the Element-Free  
503      Galerkin method, International Journal of Solids and Structures 33 (1996)  
504      3057–3080.
- 505      [6] D. Millán, A. Rosolen, M. Arroyo, Thin shell analysis from scattered points  
506      with maximum-entropy approximants, International Journal for Numerical  
507      Methods in Engineering 85 (2011) 723–751..  
508      J. S. Chen, M. Hillman, S. W. Chi, Meshfree methods: Progress made after  
509      20 Years, Journal of Engineering Mechanics 143 (2017) 04017001.
- 510      [7] D. Wang, C. Song, H. Peng, A circumferentially enhanced Hermite  
511      reproducing kernel meshfree method for buckling analysis of Kirchhoff–Love  
512      cylindrical shells, International Journal of Structural Stability and  
513      Dynamics 15 (2015) 1450090.  
514      P. Krysl, T. Belytschko, Analysis of thin shells by the Element-Free  
515      Galerkin method, International Journal of Solids and Structures 33 (1996)  
516      3057–3080.
- 517      [8] M. Behzadinasab, M. Alaydin, N. Trask, Y. Bazilevs, A general-purpose,  
518      inelastic, rotation-free Kirchhoff–Love shell formulation for peridynamics,  
519      Computer Methods in Applied Mechanics and Engineering 389 (2022)  
520      114422.
- 521      [9] J. Kiendl, K. U. Bletzinger, J. Linhard, R. Wüchner, Isogeometric shell  
522      analysis with Kirchhoff–Love elements, Computer Methods in Applied  
523      Mechanics and Engineering 198 (2009) 3902–3914.

- 524 [10] G. R. Liu, Meshfree Methods: Moving Beyond the Finite Element Method,  
 525 Second Edition, Crc Press, 2009.
- 526 ~~X. Zhang, K. Z. Song, M. W. Lu, X. Liu, Meshless methods based on  
 527 collocation with radial basis functions, Computational Mechanics 26 (2000)  
 528 333–343.~~
- 529 [11] ~~J. S. Chen, M. Hillman, S. W. Chi, Meshfree methods: Progress made after  
 530 20 Years, Journal of Engineering Mechanics 143 (2017) 04017001.~~  
 531 ~~D. Millan, A. Rosolen, M. Arroyo, Thin shell analysis from scattered points  
 532 with maximum-entropy approximants, International Journal for Numerical  
 533 Methods in Engineering 85 (2011) 723–751.~~
- 534 [12] ~~X. Zhang, Z. Chen, Y. Liu, The Material Point Method: A  
 535 Continuum-Based Particle Method for Extreme Loading Cases, Academic  
 536 Press, Oxford, 2017.~~
- 537 [13] ~~P. Suchde, T. Jacquemin, O. Davydov, Point Cloud Generation for  
 538 Meshfree Methods: An Overview, Archives of Computational Methods in  
 539 Engineering 30 (2022) 889–915.~~
- 540 [14] L. Wang, M. Hu, Z. Zhong, F. Yang, Stabilized Lagrange Interpolation  
 541 Collocation Method: A meshfree method incorporating the advantages of  
 542 finite element method, Computer Methods in Applied Mechanics and En-  
 543 gineering 404 (2023) 115780.  
 544 ~~P. Suchde, T. Jacquemin, O. Davydov, Point Cloud Generation for  
 545 Meshfree Methods: An Overview, Archives of Computational Methods in  
 546 Engineering 30 (2022) 889–915.~~
- 547 [15] L. Deng, D. Wang, An accuracy analysis framework for meshfree collocation  
 548 methods with particular emphasis on boundary effects, Computer Methods  
 549 in Applied Mechanics and Engineering 404 (2023) 115782.
- 550 [16] J. Wang, M. Hillman, Upwind reproducing kernel collocation method for  
 551 convection-dominated problems, Computer Methods in Applied Mechanics  
 552 and Engineering 420 (2024) 116711.
- 553 [17] ~~T. Belytschko, Y. Y. Lu, L. Gu, Element-free Galerkin methods,  
 554 International Journal for Numerical Methods in Engineering 37 (1994)  
 555 229–256.~~
- 556 [18] ~~W. K. Liu, S. Jun, Y. F. Zhang, Reproducing kernel particle methods,  
 557 International Journal for Numerical Methods in Fluids 20 (1995)  
 558 1081–1106.~~
- 559 [19] S. Fernández-Méndez, A. Huerta, Imposing essential boundary conditions  
 560 in mesh-free methods, Computer Methods in Applied Mechanics and En-  
 561 gineering 193 (2004) 1257–1275.

- 562 [20] X. Li, Error estimates for the moving least-square approximation and the  
 563 element-free Galerkin method in n-dimensional spaces, *Applied Numerical*  
 564 *Mathematics* 99 (2016) 77–97.
- 565 [21] J. Wu, D. Wang, An accuracy analysis of Galerkin meshfree methods ac-  
 566 counting for numerical integration, *Computer Methods in Applied Mechan-  
 567 ics and Engineering* 375 (2021) 113631.
- 568 [22] J. S. Chen, H. P. Wang, New boundary condition treatments in meshfree  
 569 computation of contact problems, *Computer Methods in Applied Mechan-  
 570 ics and Engineering* 187 (2000) 441–468.
- 571 [23] D. Liu, Y. M. Cheng, The interpolating element-free Galerkin (IEFG)  
 572 method for three-dimensional potential problems, *Engineering Analysis  
 573 with Boundary Elements* 108 (2019) 115–123.
- 574 [24] V. Ivannikov, C. Tiago, P. M. Pimenta, On the boundary conditions of the  
 575 geometrically nonlinear Kirchhoff–Love shell theory, *International Journal  
 576 of Solids and Structures* 51 (2014) 3101–3112.
- 577 [25] Y. Y. Lu, T. Belytschko, L. Gu, A new implementation of the element free  
 578 Galerkin method, *Computer Methods in Applied Mechanics and Engineer-  
 579 ing* 113 (1994) 397–414.
- 580 [26] T. Zhu, S. N. Atluri, A modified collocation method and a penalty formu-  
 581 lation for enforcing the essential boundary conditions in the element free  
 582 Galerkin method, *Computational Mechanics* 21 (1998) 211–222.
- 583 [27] S. Skatulla, C. Sansour, Essential boundary conditions in meshfree methods  
 584 via a modified variational principle: Applications to shell computations,  
 585 *Computer Assisted Mechanics and Engineering Sciences* 15 (2008) 123–142.
- 586 [28] Y. Guo, Z. Zou, M. Ruess, Isogeometric multi-patch analyses for mixed  
 587 thin shells in the framework of non-linear elasticity, *Computer Methods in  
 588 Applied Mechanics and Engineering* 380 (2021) 113771.
- 589 [29] J. Wang, G. Zhou, M. Hillman, A. Madra, Y. Bazilevs, J. Du, K. Su,  
 590 Consistent immersed volumetric Nitsche methods for composite analysis,  
 591 *Computer Methods in Applied Mechanics and Engineering* 385 (2021)  
 592 114042.
- 593 [30] J. S. Chen, C. T. Wu, S. Yoon, Y. You, A stabilized conforming nodal  
 594 integration for Galerkin mesh-free methods, *International Journal for Nu-  
 595 matical Methods in Engineering* 50 (2001) 435–466.
- 596 [31] J. S. Chen, M. Hillman, M. Rüter, An arbitrary order variationally consis-  
 597 tent integration for Galerkin meshfree methods, *International Journal for  
 598 Numerical Methods in Engineering* 95 (2013) 387–418.

- 599 [32] Q. Duan, X. Li, H. Zhang, T. Belytschko, Second-order accurate derivatives  
600 and integration schemes for meshfree methods, International Journal for  
601 Numerical Methods in Engineering 92 (2012) 399–424.
- 602 [33] D. Wang, J. Wu, An inherently consistent reproducing kernel gradient  
603 smoothing framework toward efficient Galerkin meshfree formulation with  
604 explicit quadrature, Computer Methods in Applied Mechanics and Engi-  
605 neering 349 (2019) 628–672.
- 606 [34] J. Wang, X. Ren, A consistent projection integration for Galerkin meshfree  
607 methods, Computer Methods in Applied Mechanics and Engineering 414  
608 (2023) 116143.
- 609 [35] J. Wu, X. Wu, Y. Zhao, D. Wang, A consistent and efficient method for  
610 imposing meshfree essential boundary conditions via hellinger-reissner vari-  
611 ational principle., Chinese Journal of Theoretical and Applied Mechanics  
612 54 (2022) 3283–3296.
- 613 [36] J. Wu, X. Wu, Y. Zhao, D. Wang, A rotation-free Hellinger-Reissner mesh-  
614 free thin plate formulation naturally accommodating essential boundary  
615 conditions, Engineering Analysis with Boundary Elements 154 (2023) 122–  
616 140.
- 617 [37] J. Benzaken, J. A. Evans, S. F. McCormick, R. Tamstorf, Nitsche’s method  
618 for linear Kirchhoff–Love shells: Formulation, error analysis, and verifica-  
619 tion, Computer Methods in Applied Mechanics and Engineering 374 (2021)  
620 113544.
- 621 [38] H. Dah-wei, A method for establishing generalized variational principle,  
622 Applied Mathematics and Mechanics 6 (1985) 501–509.
- 623 [39] H. Du, J. Wu, D. Wang, J. Chen, A unified reproducing kernel gradient  
624 smoothing Galerkin meshfree approach to strain gradient elasticity, Com-  
625 putational Mechanics 70 (2022) 73–100.  
626 ~~J. Kiendl, K. U. Bletzinger, J. Linhard, R. Wüchner, Isogeometric shell  
627 analysis with Kirchhoff Loveelements, Computer Methods in Applied  
628 Mechanics and Engineering 198 (2009) 3902–3914.~~
- 629 [40] R. H. MacNeal, R. L. Harder, A proposed standard set of problems to test  
630 finite element accuracy, Finite Elements in Analysis and Design 1 (1985)  
631 3–20.